CHARLES UNIVERSITY IN PRAGUE

Faculty of Science

Department of Physical and Macromolecular Chemistry

& J. Heyrovský Institute of Physical Chemistry of the CAS

Ph.D. study program:

Modelling of Chemical Properties on Nano- and Biostructures

Mgr. Kamila Riedlová

INFLUENCE OF SELECTED DRUG MOLECULES ON HUMAN TEAR FILM LIPID LAYER MODELS

STUDIUM VLIVU ZVOLENÝCH LÉČIV NA MODELECH LIPIDOVÉ VRSTVY SLZNÉHO FILMU LIDSKÉHO OKA

Doctoral Thesis

Supervisor: prof. Dr. habil. Lukasz Cwiklik, Ph.D.

Prague 2024

I hereby declare that I have completed this thesis independently under the supervision of Prof. Dr. habil. Lukasz Cwiklik, Ph.D. All publications and other sources used in this thesis have been properly cited. I also declare that this thesis has not been submitted for the award of any academic degree at any other institution.

In Prague, 13th August 2024 .....

Author's signature

Abstract: This dissertation investigates the molecular interactions of various ophthalmic drugs and pharmacologically significant compounds with models of the tear film lipid layer (TFLL) using molecular dynamics (MD) simulations. The study focuses on benzalkonium chlorides (BAKs), latanoprost (LTP), surfactant protein G (SP-G), simulated in TFLL, and the H1 peptide derived from colicin U, simulated within model lipid bilayers. MD simulations provided detailed insights into the interactions of these compounds with lipid environments. LTP was observed to integrate into the TFLL. LTP demonstrated a significant tendency to migrate and incorporate into the lipid layer, influencing the structural dynamics of TFLL. This suggests that therapeutic efficacy could be enhanced through sustained release. The behavior of BAKs in TFLL highlighted their dual role, affecting both drug delivery and tear film (TF) integrity. Our simulations showed that BAK molecules at different concentrations could disrupt TFLL, leading to changes in lipid organization and potential TF destabilization. This necessitates careful consideration of the concentration used to balance preservative efficacy with maintaining TF stability. SP-G demonstrated a stabilizing effect on TFLL. By simulating SP-G in TFLL with varying concentrations of polar lipids, it was found that SP-G could adsorb to the water-lipid interface, integrate into the lipid layer, and thereby enhance its stability. This suggests a potential of amphiphilic nanoparticles similar to SP-G for therapeutic use in treating ocular surface disorders, particularly in stabilizing the TF in conditions like dry eye syndrome. The H1 peptide showed the ability to form pores in model lipid bilayers, indicating its potential as an antimicrobial agent. Simulations and experimental liposome tests confirmed that H1 peptides could disrupt bacterial membranes, forming stable water-filled pores. This indicates their potential use in treating bacterial infections on the ocular surface. However, observed interactions and non-selective structural disruptions indicate the need for further optimization, especially in the sensitive environment of the ocular surface. The publications included in this dissertation expand our understanding of drug interactions and potential therapeutics on the ocular surface, offering valuable insights for the development of safer and more effective ophthalmic drugs and compounds.

Keywords: molecular dynamics simulations, coarse grained simulations, tear film, tear film lipid layer, latanoprost, benzalkonium chlorides (BAKs), surfactant protein G (SP-G), colicin U

Abstrakt: Tato dizertační práce zkoumá molekulární interakce různých oftalmologických léčiv a farmakologicky významných sloučenin s modely lipidové vrstvy slzného filmu (TFLL) pomocí simulací molekulové dynamiky (MD). Studie se zaměřuje na benzalkonium chloridy (BAKs), latanoprost (LTP), surfaktantový protein G (SP-G), simulované v TFLL, a H1 peptid odvozený od kolicinu U, který byl simulován v modelových lipidových dvojvrstvách. MD simulace poskytly podrobné poznatky o interakcích těchto sloučenin s lipidovými prostředími. Bylo pozorováno, že LTP se integruje do TFLL. LTP vykazoval významnou tendenci migrovat a začleňovat se do lipidové vrstvy a ovlivňovat tak strukturální dynamiku TFLL. To naznačuje, že terapeutická účinnost může být zvýšena díky postupnému uvolňování. Chování BAKs v TFLL zdůraznilo jejich dvojí roli, ovlivňující jak dodávku léčiva, tak integritu slzného filmu (TF). Naše simulace ukázaly, že molekuly BAKů při různých koncentracích mohou narušit TFLL, což vede ke změnám v lipidovém uspořádání a potenciální destabilizaci TF. To vyžaduje pečlivé zvážení používané koncentrace, aby se vyvážila účinnost konzervantu s udržením stability TF. SP-G prokázal stabilizační účinek na TFLL. Simulací SP-G v TFLL při různých koncentrací polárních lipidů bylo zjištěno, že se SP-G může adsorbovat na rozhraní voda-lipid, integrovat se do lipidové vrstvy a zvyšovat tím tak její stabilitu. Toto naznačuje potenciál amfifilních nanočástic podobných SP-G pro terapeutické využití při léčbě očních povrchových poruch, zejména při stabilizaci TF v podmínkách, jako je syndrom suchého oka. H1 peptid ukázal schopnost tvořit póry v modelových lipidových dvojvrstvách, což poukazuje na jeho potenciál jako antimikrobiálního činidla. Simulace a experimentální testy s liposomy potvrdily, že H1 peptidy mohou narušit bakteriální membrány, tvořit stabilní vodou naplněné póry. Což by mohlo poukazovat na jejich potenciální využití při léčbě bakteriálních infekcí na očním povrchu. Pozorované interakce a neselektivní strukturální narušení však ukazují na nutnost další optimalizace, zejména v citlivém prostředí očního povrchu. Publikace přiložené v této dizertační práci rozšiřují naše chápání interakcí léčiv a potenciálních léčiv na očním povrchu a poskytují cenné poznatky pro vývoj bezpečnějších a účinnějších oftalmologických léčiv a látek.

Klíčová slova: simulace molekulové dynamiky, coarse grained simulace, slzný film, lipidová vrstva slzného filmu, latanoprost, benzalkonium chloridy (BAKs), surfaktantový protein G (SP-G), kolicin U

List of publications

Publications that are part of this dissertation:

- **Riedlová, K.**, Saija, M. C., Olżyńska, A., Vazdar, K., Daull, P., Garrigue, J. S., & Cwiklik, L. (**2023**). Latanoprost incorporates in the tear film lipid layer: An experimental and computational model study. *International Journal of Pharmaceutics, 645, 123367.*

- **Riedlová, K.**, Saija, M. C., Olżyńska, A., Jurkiewicz, P., Daul, P., Garrigue, J. S., & Cwiklik, L. (**2023**). Influence of BAKs on tear film lipid layer: In vitro and in silico models. *European Journal of Pharmaceutics and Biopharmaceutics, 186, 65-73.*

- Schicht, M., **Riedlová, K.**, Kukulka, M., Li, W., Scheer, A., Garreis, F., ... & Bräuer, L. (**2022**). The potential role of SP-G as surface tension regulator in tear film: From molecular simulations to experimental observations. *International Journal of Molecular Sciences, 23(10), 5783.* **The first two authors share first authorship**.

- **Riedlová, K.**, Dolejšová, T., Fišer, R., & Cwiklik, L. (**2022**). H1 helix of colicin U causes phospholipid membrane permeation. *Biochimica et Biophysica Acta (BBA)-Biomembranes, 1864(4), 183866.*

Publications that are not part of this dissertation:

- Golda-Cepa, M., **Riedlová, K.**, Kulig, W., Cwiklik, L., & Kotarba, A. (**2020**). Functionalization of the parylene c surface enhances the nucleation of calcium phosphate: Combined experimental and molecular dynamics simulations approach. *ACS applied materials & interfaces, 12(11), 12426-12435.*

- **Riedlova, K.**, Melcrova, A., Olzynska, A., Daull, P., Garrigue, J. S., & Cwiklik, L. (**2019**). Influence of benzalkonium chloride on tear film lipid layer stability: A molecular level view by employing in silico modeling. *Modeling and Artificial Intelligence in Ophthalmology, 2(3), 36-42.*

- **Riedlová, K.**, Nekardova, M., Kačer, P., Syslova, K., Vazdar, M., Jungwirth, P., ... & Cwiklik, L. (**2017**). Distributions of therapeutically promising neurosteroids in cellular membranes. *Chemistry and physics of lipids, 203, 78-86.*

Conferences:

- 2017: EJTEMM2017 (5th European Joint Theoretical/Experimental Meeting on Membranes), Krakow, Poster: Structure of pore-forming colicins in POPC membrane
- 2018: Wroclaw-Prague Seminar on Biophysics of Lipids, Wroclaw, Talk: Pore-forming colicins in model lipid membranes
- 2018: Levi IV (Biologically relevant Membrane and Monolayer related processes), Nové Hrady, Talk: Pore-forming colicins behavior in model lipid membranes
- 2018: EJTEMM2018 (6th European Joint Theoretical/Experimental Meeting on Membranes), Helsinky, Poster: Influence of benzalkonium chlorides on human tear film lipid layer models

Contents

1. Introduction

1.1 Biological background

Pharmaceutical science today focuses on identifying small molecules that benefit and safeguard organism health, alongside developing methods for their effective delivery to action sites. This encompasses drug design and drug delivery strategies. Even drugs suitable for specific uses can inadvertently affect unintended areas, causing significant undesired damage and side effects. The ideal drug design balances efficacy, toxicity, and solubility [1].

Nowadays, diseases can be treated by applying drugs in different ways: orally, rectally, parenterally, topically, sublingually, by inhalation, and so on [2, 3]. This dissertation addresses topically applied ophthalmic drugs or pharmacologically significant compounds also administered via this route. Topical application refers to the direct application of a drug to the action site, such as the skin or eyes [2, 3]. Ocular drug administration is challenging due to the eye's complex structure. Traditional methods like eye drops and ointments encounter problems because they are easily removed by tears or eye protective mechanisms and often require complex drug carriers to maintain efficacy [4, 5]. Successful topical application requires a stable chemical environment to accommodate multiple compounds with varying physicochemical properties. The advantages include reduced toxicity due to direct application and avoidance of systemic metabolic processes [6, 7]. However, even when correctly applied, eye drops can sometimes result in unwanted systemic absorption due to high concentrations of active drugs [8]. One of the methods to improve the properties of eye drop products is the use of lipid-based drug nanocarriers, which are increasingly used for their low toxicity and effective delivery [4, 5, 9, 10].

1.1.1 Tear film and its layers

The tear film (TF) is essential for maintaining corneal health, providing nutrition, lubrication, and protection against infections. The stability of the TF ensures consistent vision. It is structured into three distinct layers, each with specific functions [11, 12, 13, 14]:

- **Inner mucin layer:** Composed mainly of mucins, which are glycoproteins (sugar-

rich glycosylated proteins) critical for protecting the cornea's surface. This layer ensures the adhesion of the TF to the eye's surface, facilitating the smooth and even spread of the aqueous layer after blinks, thereby enhancing optical quality and providing a barrier against pathogens [13, 14, 15].

- **Middle aqueous layer:** This layer constitutes a high percentage of the tear volume and is responsible for keeping the eye's surface moist and providing an optically smooth surface for light refraction. It contains a variety of components such as electrolytes, vitamins, glucose, lactoferrin, lysozyme, and immunoglobulins, which are vital for immune defense and nutrient transport to corneal cells [13, 14, 16].

- **Outer lipid layer:** Predominantly composed of polar and non-polar lipids, this thin layer significantly lowers the TF's surface tension, reducing evaporation and providing hydration to the eye surface. It also serves as the primary interface for various ophthalmic drugs and the external environment, thus playing a crucial role in drug efficacy and eye protection [11, 14, 17].

1.1.2 Blinking dynamics and tear film renewal

Blinking serves as a critical protective mechanism for the eye surface and facilitates several key processes: mechanical cleaning of the eye surface, tear distribution, and TF maintenance and restoration. During a blink, the upper eyelid moves downward while the lower eyelid rises, creating a sweeping motion that helps remove debris and foreign particles. This action effectively clears the eye surface by pushing tears toward the inner corner of the eye, away from the central visual field [13, 18, 19].

Blinking temporarily alters the thickness of the TF, typically ranging from 4 to 9 μm [20]. This change in thickness ensures the even distribution of the TF across the cornea, which is critical for maintaining hydration and optical clarity. Immediately after blinking, the TF rapidly thins and spreads across the corneal surface. This rapid restoration is crucial to prevent excessive tear evaporation, which can compromise the mucin layer's ability to adhere to the eye surface. If the TF evaporates too quickly, the eye becomes vulnerable to external environmental factors, potentially leading to bacterial infections and other ocular damage [13, 14, 20, 21].

Disruptions in the TF, whether due to abnormalities in its composition, blink rate, or various other conditions, can lead to dry eye condition. This disease is characterized by a stability deficient TF that fails to adequately protect and nourish the eye surface, leading to irritation, inflammation, and, if untreated, more severe ocular damage and visual disturbance. Dry eye disease is a multifactorial, and its complexities require a comprehensive understanding to develop effective treatments [16, 22, 23, 24].

Current therapies aim to restore the ocular surface environment to its optimal state. They often involve the use of various eye drops designed to supplement the natural TF, though the specific mechanisms by which these components exert their beneficial effects, as well as their potential drawbacks, are not yet fully understood. Moreover, the role of different proteins in stabilizing the TF over the long term remains an area of active research, highlighting the need for ongoing studies in this field [13, 16].

1.1.3 Lipophilic ophthalmic active drugs and preservatives

The treatment of ocular conditions often involves the use of lipophilic drugs due to their ability to penetrate lipid-rich tissues [10, 25]. This section of the thesis delves into the specifics of such medications, focusing on latanoprost used for glaucoma [26] treatment [27, 28], alongside the role of preservatives which, while necessary for maintaining drug stability and efficacy, can have adverse effects on ocular health [29].

Latanoprost

Latanoprost (LTP), a prostaglandin F2α analogue, is a lipophilic ester prodrug primarily used in the treatment of ocular hypertension and open-angle glaucoma [28, 30]. Presently, the main route of LTP administration is in the form of topical eye drops. It operates by increasing the outflow of aqueous fluid from the eye through the uveoscleral pathway, effectively reducing intraocular pressure. Once administered, LTP is hydrolyzed by esterases in the cornea into its active form, LTP acid. This acid is a potent agonist at the prostaglandin F receptor, enhancing the permeability of the sclera and subsequently increasing aqueous outflow, which leads to a decrease in intraocular pressure and helps slow the progression of glaucoma. Due to its efficacy and safety profile, LTP is often the first-line treatment for these conditions [27, 28, 30]. Understanding the molecular

behavior of LTP within the human eye is crucial for optimizing its delivery and efficacy.

The activation of the prostaglandin F receptor by LTP acid not only facilitates fluid drainage but also involves complex interactions with other ocular tissues, which are under ongoing investigation to further elucidate the drug's therapeutic mechanisms.

Preservatives in ophthalmic solutions

Preservatives are essential components of many ophthalmic solutions, tasked with preventing microbial contamination over the usage period of the product. However, the inclusion of these chemicals can lead to complications, particularly with long-term use. The most commonly used group of preservatives in eye solutions comprises benzalkonium chlorides (BAKs), which are quaternary ammonium compounds known for their effective antimicrobial and surface-active properties [29, 31].

BAKs are mixtures of alkylbenzyldimethylammonium chlorides with alkyl chains ranging from C8 to C18. For instance, BAK-C12 is known as benzododecinium chloride, and BAK-C16 as cetalkonium chloride [29, 32, 33]. The chemical structures of these compounds are detailed in the Methodology section 3.1.3, Figure 3.3.

These compounds assist in stabilizing the TF and enhancing the solubility of active drugs. However, they have been associated with several adverse effects, such as TF instability, disruption of the corneal epithelial barrier, and potential damage to deeper ocular tissues. The detrimental effects of BAKs are believed to stem from their surfactant properties, which can disrupt cellular membranes and promote inflammatory responses. The toxicity of BAKs can vary depending on their concentration and the length of exposure, with mechanisms involving the disruption of lipid layers and protein structures within the TF, leading to increased evaporation and cellular toxicity [29, 34].

The ongoing use of BAKs has sparked debate over their safety, prompting research into less harmful alternatives that maintain microbial control without damaging ocular tissues [29, 34]. In response to these concerns, alternative preservatives are being developed to reduce ocular surface damage while still providing effective antimicrobial protection. These alternatives aim to be less cytotoxic and more biocompatible with the ocular surface, ensuring patient comfort and compliance.

This work investigates the effects of different BAK chain lengths: -C16, -C12, and

-C8 on TF structure and ocular surface integrity. By understanding the interactions of these compounds with the TF at the ocular surface, we can better design formulations that minimize adverse effects while maximizing therapeutic efficacy. This will enable the development of safer, more effective ophthalmic treatments that reduce the risk of adverse effects and improve patient outcomes.

1.1.4 Tear film proteins and their role in ocular health

The TF's outer lipid layer (TFLL) is crucial for ocular surface protection, involving a complex interplay of lipids and proteins. This layer not only prevents excessive evaporation but also shields the eye from microbial colonization. Among the proteins integral to the TFLL are well-known antibacterial agents like lactoferrin and lysozyme, as well as surface-active proteins, which play pivotal roles in maintaining the stability and functionality of this barrier [14, 35].

One significant surface-active protein is Surfactant protein G (SP-G) [36, 37], noted for its unique structure with amphipathic residues, hence containing both hydrophobic and hydrophilic regions. This structural feature allows SP-G to interact effectively with both the aqueous and lipid components of the TF, suggesting a potential stabilizing role. SP-G is not only produced in ocular surface tissues but also by lung alveoli, highlighting its multifunctional nature across different body sites. The protein's role in the ocular environment extends to immunological functions, potentially enhancing the eye's defense mechanisms against pathogens. The importance of SP-G in the context of dry eye disease, a condition often accompanied by a weakened TFLL and associated tear deficiency, cannot be overstated. Its ability to interact with and stabilize the lipid layer may prove crucial in therapeutic strategies aimed at restoring TF integrity and function [36, 37, 38, 39].

1.1.5 Ophthalmology peptide antibiotics

The exposed nature of the ocular surface to environmental factors necessitates robust antimicrobial defenses to prevent infections that could impair vision. In ophthalmic pharmacology, the strategies employed to enhance these defenses include the development of peptide antibiotics. Peptide antibiotics are typically small, amphipathic molecules comprising both polar and non-polar amino acids, enabling them to insert into and disrupt

bacterial membranes effectively. The strategic use of these peptides in ophthalmology stems from their ability to target and neutralize pathogens without the resistance issues often associated with traditional antibiotics [40, 41].

An example in our antibiotic-related research in the ophthalmic context was the H1 peptide derived from colicin U [42, 43, 44], a bacteriocin known for its potent antimicrobial activity. The amphipathic nature of the H1 peptide makes it particularly effective at interacting with the lipid components of microbial membranes. Additionally, it may lead to specific interactions with the lipid layer of the tear film. Therefore, the incorporation of such peptides into treatment regimens for ocular infections could offer a promising avenue for enhancing the antimicrobial efficacy of eye drops and other topical treatments.

1.2 Computational background

Computational biophysics and chemistry methods are a vital tool for understanding molecular interactions, crucial for advancements in medicine and pharmacology. They can reveal system behaviors that are challenging to capture experimentally [1]. Molecular mechanics (MM) models molecules as atoms represented by spheres linked by springs, embodying bonds and interatomic forces [1, 45]. This approach uses quantum theoretical and empirical data to parameterize interactions, aiding in the understanding of intra and intermolecular forces [46].

Molecular Dynamics (MD) simulations, based on classical mechanics, are essential for studying real-time atomic and molecular pharmacological interactions [1]. By applying Newton's laws, MD simulations compute particle trajectories, enhancing our understanding of complex biological mechanisms at the molecular level.

1.2.1 Fundamentals of all-atom MD simulations

At the core of MD simulations is Newton's second law (Eq. 1.1), which calculates particle accelerations based on the forces acting on them.

$$\mathbf{F} = m\mathbf{a} \tag{1.1}$$

Eq. 1.1: Newton's second law, where $\mathbf{F}$ denotes the force exerted on a particle, m its mass, and $\mathbf{a}$ its acceleration.

These forces are derived from the negative gradients of potential energy (Eq. 1.2) [47].

$$\mathbf{F} = -\nabla V(\mathbf{r}) \tag{1.2}$$

Eq. 1.2: Definition of force in a conservative field, where V($\mathbf{r}$) symbolizes the potential energy and $\mathbf{r}$ the coordinates of the particles.

Once the acceleration of each particle is determined, it is used to update the particle's velocity and, consequently, its position in space over a small time step. This process of updating particle positions and velocities is iterative. As new particle positions are calculated, the potential energy and corresponding forces are reassessed. This cyclic process is repeated over numerous time steps, predicting particle trajectories and elucidating atomic movements over time [47, 48, 49].

Force fields in MD simulations

All-atom MD simulations use force fields (FFs) to describe interactions between every atom, including bond stretching, angle bending, dihedral angles, and non-bonding interactions like van der Waals forces and electrostatic interactions [50, 46, 51]. A generalized FF equation is:

$$U = U_{\text{bonds}} + U_{\text{angles}} + U_{\text{dihedrals}} + U_{\text{non-bonded}} \tag{1.3}$$

Eq.1.3: MM generalized force field, where U_{bonds} represents energy contributions from bond stretching, U_{angles} from angle bending, and $U_{dihedrals}$ from dihedral rotations, while $U_{non-bonded}$ accounts for non-covalent interactions. The equation was written according to [51].

For a more granular view of the FF parameters (Eq. 1.4) :

$$\begin{aligned} U = &\sum_{\text{bonds}} k_l(l - l_0)^2 + \sum_{\text{angles}} k_\theta(\theta - \theta_0)^2 + \sum_{\text{dihedrals}} k_\phi[1 + \cos(n\phi - \gamma)] \\ &+ \sum_{\text{impropers}} k_\omega(\omega - \omega_0)^2 + \sum_{i<j} \epsilon_{ij} \left[\left(\frac{r_m}{r_{ij}} \right)^{12} - 2 \left(\frac{r_m}{r_{ij}} \right)^{6} \right] + \sum_{i<j} \frac{q_i q_j}{4\pi\epsilon_0 r_{ij}} \end{aligned} \tag{1.4}$$

Eq. 1.4: Parameters of modern MM force field. The first sum represents the bond energy, where k_l is the bond stiffness, l is the current bond length, and l_0 is the equilibrium bond length. The second sum expresses the angle energy, with k_θ as the angle stiffness, θ as the current angle, and θ_0 as the equilibrium angle. The third sum corresponds to the dihedral energy, where k_ϕ is the dihedral angle constant, n represents periodicity, ϕ is the

dihedral angle, and γ is the phase shift. The fourth sum accounts for the improper dihedral energy, where k_ω is the improper angle stiffness, ω is the current improper dihedral angle, and ω_0 is the equilibrium improper dihedral angle. The fifth sum accounts for the van der Waals potential energy for non-bonded interactions, quantified through the Lennard-Jones potential. Here, ϵ_{ij} represents the depth of the potential well, indicating the strength of attraction between particles i and j, r_m is the distance at which the potential reaches its minimum, and r_{ij} is the actual distance between particles i and j. The expression $\left(\frac{r_m}{r_{ij}}\right)^{12}$ accounts for the repulsive force due to Pauli repulsion at short ranges, whereas the term $-2\left(\frac{r_m}{r_{ij}}\right)^{6}$ represents the attractive force that decays with distance. This dual component function captures the essential features of molecular interactions over a range of distances. The final term represents the Coulomb interaction between charged particles, where q_i and q_j are the charges of the particles i and j, ϵ_0 is the vacuum permittivity, and r_{ij} is the distance between particles i and j [46, 52]. The equation was taken from [53] and modified.

Limitations of all-atom MD simulations

Despite their effectiveness, MD simulations are limited by approximations in potential energy models and initial uncertainties in particle positions, often derived from protein crystallography data, and velocities. Additionally, computational limitations restrict the time scale and size scale detail of these simulations. Standard MD simulations offer detailed insights at the all-atom level typically on nanosecond to microsecond time scales for systems up to 20 nm in size [1, 50]. However, many biological phenomena require analysis over more extended temporal and spatial scales. Coarse-grained (CG) simulations enable the study of larger systems on the order of micrometers and longer time scales, reaching up to and beyond microseconds [52].

1.2.2 Coarse-grained molecular dynamics simulations

In CG simulations, groups of atoms are represented by single particles, averaging out atomic details and simplifying the molecular model [52, 54]. This method reduces system granularity and expedites simulation times [1].

The mathematical formulation of CG FF varies depending on the specific coarse-graining strategy employed. This approach involves translating detailed atomistic properties into a more generalized CG representation, focusing on capturing essential physicochemical characteristics [52, 55, 56].

Although this approach sacrifices all-atom granularity, it is effective for exploring fundamental molecular behaviors such as localization, orientation within lipid bilayers or multilayers, and interactions with specific molecular targets, which are crucial for pharmacological research. Because of the various levels of time and size scales of the systems studied in this thesis, both all-atom and CG approaches were used.

1.2.3 MD simulation of drugs in combination with lipid mono-, bi-, and multilayers

MD simulations offer valuable insights into the adsorption, diffusion, and permeation of drugs through lipid mono-, bi-, and multilayers, which are critical for understanding drug efficacy and delivery mechanisms. For instance, all-atom MD simulations can model the precise interactions between drug molecules and lipid membranes, revealing how drugs integrate into or disrupt lipid structures [1, 50].

Moreover, MD simulations are pivotal in the design and optimization of new drugs and nanocarriers. By simulating the interaction of drug molecules with potential delivery vehicles, one can identify optimal formulations and improve drug stability and bioavailability. These simulations help in predicting the pharmacokinetic and pharmacodynamic properties of drugs, enabling the fine-tuning of molecular structures for better therapeutic outcomes [1, 50, 57].

In the context of nanocarriers, MD simulations allow the exploration of how drug-loaded nanoparticles interact with cell membranes or other biological structures (e.g., TFLL), facilitating targeted drug delivery and controlled release. This level of detailed molecular insight is crucial for developing advanced drug delivery systems that can overcome biological barriers and deliver therapeutic agents more efficiently [1, 50, 57].

1.2.4 Technical aspects of molecular dynamics simulations

MD simulations can be realized by several computational packages, each offering unique capabilities and optimizations. Prominent among these are NAMD [58], AMBER [59], CHARMM [60], and GROMACS [61]. In my research, I have exclusively utilized GROMACS, a robust and freely available software suite initially developed by the Biophysical Chemistry department at the University of Groningen [62] and subsequently by teams at the Royal Institute of Technology and Uppsala University in Sweden [63]. GROMACS is accessible through its official website `www.gromacs.org` and its source code can be found on GitHub `https://gitlab.com/gromacs/gromacs`.

System preparation and energy minimization

Upon defining the coordinates and FFs for the system components, an initial step of energy minimization is performed using the steepest descent algorithm, typically over 1 000 steps [48, 49, 64]. This process reduces van der Waals clashes and excessive interatomic forces, stabilizing the system for dynamic simulation.

Equilibration and statistical ensembles

Following energy minimization, the system undergoes equilibration under defined thermodynamic conditions, particularly controlled temperature and pressure using the NPT (isobaric-isothermal) ensemble [48, 65]. This ensemble maintains the number of particles (N), pressure (P), and temperature (T) constant, aligning simulation conditions with laboratory environments. The NPT ensemble is preferred for most protein production simulations, but the NVT (canonical) ensemble is sometimes used for short-term protein equilibrations [66, 67]. The NVE (microcanonical) ensemble is less commonly used due to its conservation of total system energy, which can lead to undesirable temperature increases and potential denaturation of proteins [48, 68].

In our studies involving pharmacologically interesting molecules and the TFLL, we utilized the NVT ensemble due to its ability to maintain a constant volume. This was crucial as our simulation results were correlated with experimental measurements that typically operate at defined area per polar lipid (APPL). The NVT ensemble allowed us to keep the simulation box fixed, ensuring that the volume remained consistent with the

experimental conditions and providing reliable data for comparative analysis.

Equilibrium and nonequilibrium simulations in MD studies

Equilibrium MD simulations are particularly advantageous in studying drug interactions with lipid membranes, as they provide a stable environment to observe the natural behavior of the system over time. By offering insights into the structural and dynamic properties of these systems under stable conditions, equilibrium MD simulations play a vital role in advancing pharmaceutical research [69, 1, 50].

In our research, we used equilibrium MD simulations to sample the behavior of a potentially antimicrobial peptide within a lipid membrane. These simulations allow us to understand how the peptide integrates into the membrane. Equilibrium simulations are also beneficial for studying the interactions of drugs with lipid-based delivery systems, such as lipid bilayers and vesicles.

In the study of drug interactions with lipid multilayers, nonequilibrium molecular dynamics (NEMD) simulations [70] play a critical role. These simulations are designed to observe system behaviors under conditions far from equilibrium, capturing transient states, kinetic processes and initial interactions that are often missed in equilibrium studies [70, 69].

In our research, the initial interactions of drugs with the lipid layer of the TF were studied as a non-equilibrium process, mimicking the interactions of TF with the components of eye drops. NEMD simulations help in understanding how drugs penetrate and disrupt lipid structures. These simulations provide insights into the mechanisms driving drug adsorption, insertion, and the subsequent structural rearrangement of the lipid structures.

2. Objectives of this study

The primary aim of this dissertation is to elucidate the molecular-level interactions between various ophthalmic drugs, excipients, and drug carriers, and a model of the lipid layer of the human eye tear film (TFLL) or model lipid membranes. This study primarily employs molecular dynamics (MD) simulations to explore the dynamics of these pharmacologically significant compounds within our model environment. The molecular insights gained from these simulations are complemented by data obtained through experimental efforts conducted by our research group and collaborating laboratories. The research was divided into several focused sub-objectives:

- **Impact of latanoprost on the tear film:** This study included an examination of the effects of latanoprost (LTP) on the TFLL. Despite the clinical importance of LTP, there have been few simulation studies involving its interaction with the TF. Our study aimed to comprehensively understand the molecular interactions between LTP and TFLL, considering reports suggesting that prolonged use of LTP may lead to adverse effects.

- **Study of preservatives in eye drops:** The other part of the research was dedicated to investigating the molecular nature of surface-active substances such as BAKs (CKC, BAK12, BAK8), commonly used as preservatives in eye drops. These substances could potentially disrupt the functional integrity of the TF. The goal was to analyze their behavior and identify any that could be implicated in reducing the tear film's effectiveness.

- **Investigation of surfactant proteins:** Following the study of BAKs, attention shifted to a newly identified surfactant protein, SP-G, which lacks sequence or structural similarities to other known surfactant proteins. The interactions of SP-G with the lipid system in our model were studied to understand its role in the human TF, potentially contributing to treatments for dry eye syndrome.

- **Peptide interaction studies:** Another focus of the research was on a novel peptide, H1, derived from the C-terminal domain of colicin U. This peptide was hypothesized to disrupt lipid membranes, and its potential as an antimicrobial agent

was explored. The objective was to confirm its antimicrobial efficacy, decipher the mechanism of its action, and, following positive results, extend the MD simulations to include interactions within the ocular environment. This was driven by the potential application of H1 peptide as a novel antibiotic for treating bacterial colonization on the ocular surface.

This research was conducted within the Computational Chemistry Department at the J. Heyrovský Institute of Physical Chemistry of the Academy of Sciences of the Czech Republic, v.v.i., under the supervision of Prof. Dr. habil. Lukasz Cwiklik, Ph.D. The collaborative nature of this work involved a comprehensive exploration of interactions in ophthalmic pharmacology, using both computational and experimental methodologies to advance our understanding of drug interactions at the ocular surface. However, my contributions were exclusively focused on the computational part of these studies, employing molecular dynamics simulations.

3. Methods

In this study, I adopted a dual approach in MD simulations, utilizing both CG and all-atom models to investigate the behavior of ophthalmic compounds and peptides at different scales of molecular interactions.

We conducted CG MD simulations of LTP, BAKs, and SP-G to explore their interactions with models of the lipid layers of the human eye TF. The CG approach allowed for the examination of the compounds' effects over extended time scales and larger system sizes, providing insights into their behavior within the tear film's lipid matrix. Our work also involved detailed all-atom MD simulations of the peptide H1, derived from the CTD of colicin U.

In this chapter, I will briefly describe how we prepared the systems and the types of systems I studied. Detailed parameters of all production MD simulations, such as the settings of the barostats, thermostats, cutoffs, integrator parameters, etc., can be found in the attached Publications I-IV.

3.1 CG MD simulations of pharmacologically relevant compounds in TFLL

For all CG MD simulations, we utilized the MARTINI FF version 2.2 [56, 54, 71, 72], which models 3-4 atoms as a single, larger particle [1, 54]. For compounds not included in the standard MARTINI library, we developed the FFs ourselves. MARTINI FF was chosen for its good performance for lipid systems, including our previous TFLL studies, its compatibility with GROMACS, and for its ease of use.

3.1.1 CG representation of an in silico model of TFLL

The TFLL models employed were similar to those used in our previous computational studies of the TF [73, 74]. The modeling process involved placing a water layer in the simulation box expanded along the z-dimension, creating two water-vacuum interfaces. At each interface, a complex lipid film was added. A 20 nm vacuum layer was maintained

above the non-polar components. This configuration aimed to emulate the natural multi-layered structure of the human eye's lipid film.

The model lipid film consisted of a thin layer of polar lipids and a thicker layer of non-polar lipids, with a compositional ratio of 1:4, determined based on lipidomic analyses of human tears [75, 76, 77, 78]. The polar layer contained exclusively palmitoyl-oleoyl-phosphatidylcholine (POPC). Our previous work, not included in this dissertation, also considered a mixture of polar lipids [32]. The non-polar layer comprised equal molar ratios of cholesteryl erucate (CE) and behenyl oleate (BO). Figure 3.1 illustrates the chemical structure and CG representation of these lipids.

The FFs for BO and CE lipids in our TFLL model were prepared using MARTINI version 2.2, specifically adapting the MARTINI FF for cholesteryl oleate to suit our needs [79, 56]. The typical simulated system comprised approximately 90 000 water beads (water component), 727 POPC molecules (polar lipid component), and 1 250 molecules each of BO and CE (non-polar lipid components). Given the dual multilayer configuration, the total lipid count was effectively doubled. The simulation box dimensions were 22 $\times$ 22 $\times$ 104 nm^3, with the area per polar lipid (APPL) headgroup typically equal to 0.62 nm^2 [74], a metric closely aligned with experiments.

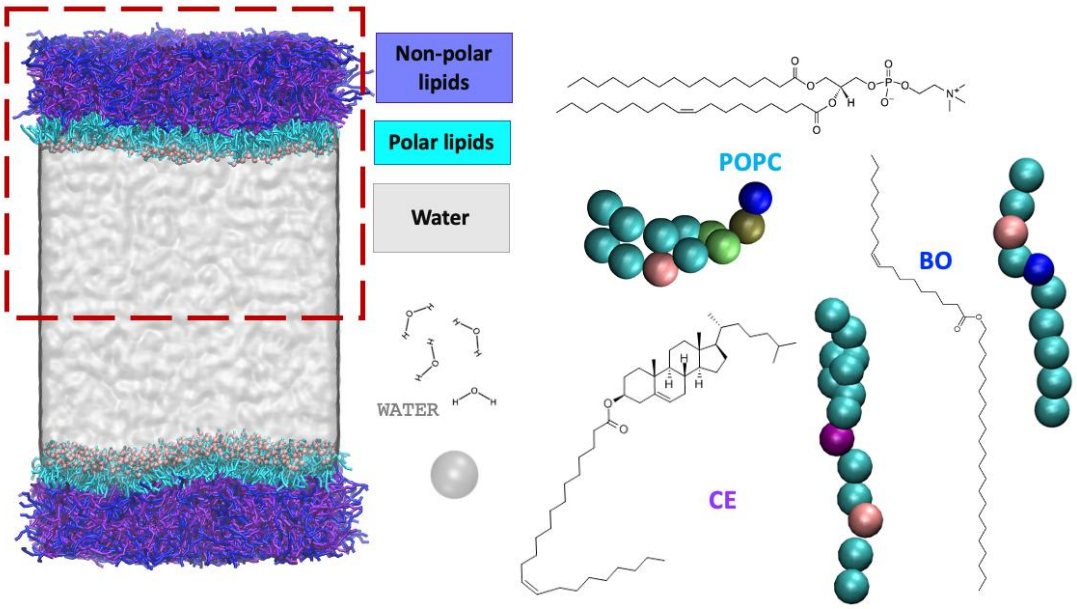

Figure 3.1: Basic model of our TFLL, visualized using VMD with the *cg_bonds-v5.tcl* script from the MARTINI website (available at `http://www.cgmartini.nl/index.php/tools2/visualization`, 24.4.2024) for displaying elastic network bonds. Color coding: BO - dark blue, CE - violet, POPC - cyan, PO_4 of POPC - pink, WATER - silver. Individual lipids in the CG representation are depicted using the VdW drawing method, colored by "Name". One MARTINI water bead corresponds to four all-atom water molecules.

This system was initially equilibrated over several hundred nanoseconds before being used for the CG MD simulation studies of LTP molecules, BAKs, and SP-G protein. The data of our analyses are typically presented for only one lipid multilayer (as depicted in Figure 3.1), specifically the one directly interacting with the introduced drug molecules.

3.1.2 CG MD simulations of Latanoprost in the TFLL

We developed the FF and CG representations of LTP using the MARTINI library version 2.2 [56]. The chemical structure, all-atom 3D coordinates, and our CG representation of LTP are illustrated in Figure 3.2.

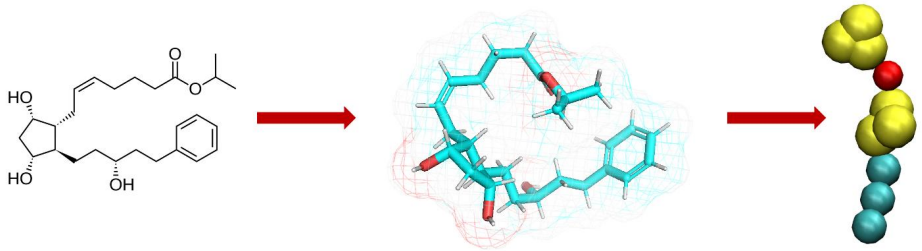

Figure 3.2: Chemical structure, all-atom 3D coordinates, and CG representation of LTP. The all-atom representation was visualized using PyMOL [80], while the CG representation of the MARTINI beads was visualized in VMD [81].

Multiple systems were prepared for the foundational CG MD study of LTP across various TFLL environments at 310 K. In a simple aqueous setup, we placed 50 molecules of LTP (also 25 or 10 LTP molecules) in random orientation among 5 000 MARTINI water beads using Packmol software [82]. This was followed by energy minimization and approximately 80 ps of equilibration in the NPT ensemble, resulting in a final box size of $9 \times 9 \times 9$ nm^3. During this phase, we utilized an isotropic Berendsen barostat [83] at a pressure of 1 bar and a high equilibration temperature of 400 K to prevent immediate LTP aggregation in water. Subsequently, we expanded the z-dimension of the box, adding an air-water interface to the existing system. After about 100 ps of equilibration, the simulation box dimensions adjusted to $9 \times 9 \times 15$ nm^3. Several scenarios were explored, including starting with LTP already aggregated in water and with LTP molecules initially dispersed. In both instances, aggregation occurred at the surface; therefore, only one representative CG MD simulation is detailed in the results.

LTP was added into our standard TFLL model in two distinct manners: either within the water phase or directly into the air environment above the TFLL. For the aqueous phase insertion, we replaced a segment of the original water molecules with a cube of

water containing LTP molecules. For the air-phase insertion, LTP aggregate was added directly to the TFLL air environment, followed by simulation.

Additional simulations involved incorporating LTP into the TFLL environment with varying concentrations of the polar lipid component. To simulate these scenarios, we removed 20 % of the original POPC layer and inserted 50 molecules of LTP. Adjustments in lipid quantity were made to accommodate the pressure changes induced by LTP adsorption.

These systems (two lipid environments) comprised 50 LTP molecules, 1 454 POPC molecules, and 2 500 molecules each of BO and CE, with 87 354 water beads. Variants with a reduced POPC concentration contained 582 POPC molecules in one lipid environment, and 727 in the second opposite lipid environment.

Water-only and air-water LTP systems underwent simulation for 1 microsecond. The TFLL system with externally added LTP continued for up to 12 microseconds due to the slow equilibration observed through contact number analysis. Conversely, the LTP system added to the aqueous phase of the TFLL equilibrated more rapidly, completing in 5 microseconds. The modified LTP model with 20 % fewer lipids was simulated over 1.6 microseconds.

3.1.3 Systems of BAKs in the TFLL

As BAK molecules are not included in the standard MARTINI library, additional FF parameters were developed specifically for this study. These parameters are accessible at `https://zenodo.org/deposit/7515840`. Figure 3.3 displays the chemical structure and CG representation of the studied BAK compounds.

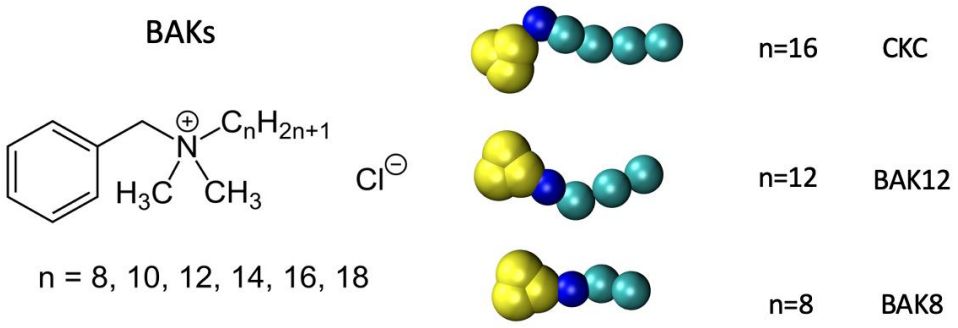

Figure 3.3: The chemical structure and CG representation of BAK compounds visualized in VMD [81] using the VdW drawing method for MARTINI beads.

Several simulation systems containing BAK8, BAK12, and CKC molecules at various concentrations were prepared. For CG MD simulations in both aqueous environments and water-vacuum interfaces (with vacuum representing the air environment), BAKs were prepared at concentrations approximately equating to 20 mmol, 40 mmol, and 200 mmol. The number of water MARTINI beads across all simulations was 49 272. The system also contained counterions for electroneutrality. The constant simulation box dimension was $19 \times 19 \times 19$ nm^3 and a temperature of 310 K. To simulate the interaction of BAK molecules at the water-air interface, the z-dimension of the simulation box was expanded, resulting in a box size of $19 \times 19 \times 60$ nm^3.

Additional systems were prepared with varying concentrations of the polar lipid component in the TFLL, specifically at BAK concentrations of 40 mmol and 150 mmol. For the higher concentration scenario, a small cube of water was replaced by a cube of BAKs in water at the desired concentration within the water phase of the TFLL. Conversely, to achieve a lower concentration of BAKs in the TFLL, we reduced the percentage of POPC lipids on both sides of our model and supplemented it with BAKs. Both systems underwent brief equilibration followed by production runs. The system with a lower concentration of POPC included 2×581 POPC molecules, while the higher concentration system contained 2×727 POPC molecules. The number of CE and BO molecules corresponded to $2 \times 1\,250$ for each, in both setups. "Twice" implies two lipid environments connected via a water cube, though interactions occurred with only one layer. The number of water beads was 66 387 (higher concentration) in the former and 89 706 in the latter setup (lower concentration).

All CG MD simulations of BAKs in water or at the water-air interface were extended to a duration of 1 microsecond to ensure the attainment of equilibrium behavior, a necessity given the complexity and dynamic nature of the systems studied. For TFLL simulations, trajectories were computed up to 3 microseconds.

3.1.4 Systems of SP-G in the TFLL

The all-atom coordinates of SP-G, available in the PMDB [84] (PMDB ID PM0078341 [36, 37]), were converted to CG coordinates and force fields using the *martinize.py* script, version 2.6, from the developer's GitHub repository `https://github.com/cgmartini/`

`martinize.py`. The DSSP program [85] was utilized to preserve the secondary structure during this process. Figure 3.4 illustrates the CG representation of the SP-G protein.

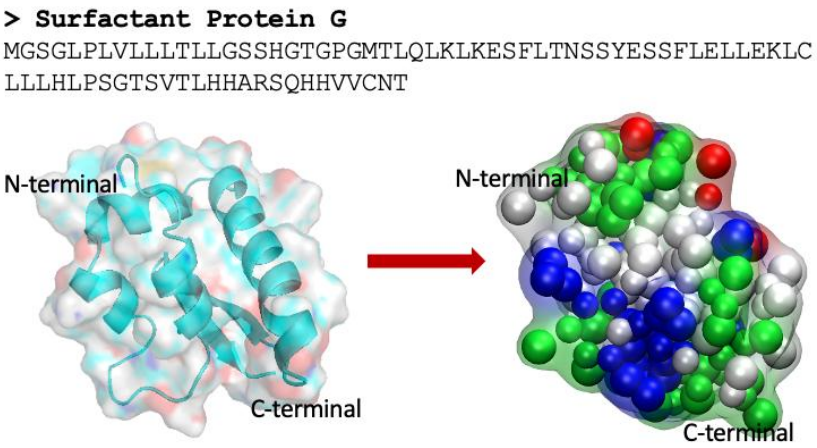

Figure 3.4: SP-G amino acid sequence in FASTA format and the structure of the SP-G protein in both all-atom and CG resolutions. Left part: All-atom structure of SP-G visualized with PyMOL [80], right part: CG representation visualized with VMD [81], colored by residue type. The all-atom structure was sourced from PMDB [84] under ID PM0078341 [36, 37].

Several replica simulation systems were prepared. As a control, a basic system consisting of a single SP-G protein with 5 000 MARTINI water beads was prepared. This system underwent a 1 000-step minimization using the steepest descent algorithm [48, 49] and was equilibrated in the NPT ensemble starting from a lower temperature of 30 K.

In subsequent CG MD simulations, a single molecule of SP-G was added into the water phase of the TFLL to monitor its adsorption on the TFLL during the simulation. We also performed several replication simulations with increased SP-G protein in TFLL. Additional CG MD simulations adjusted the number of POPC molecules in both multilayers, simulating less densely packed interfaces. CG MD simulations of lateral compression of the film were conducted by activating the pressure coupling algorithm, setting the pressure on the acting side to 15 bar.

3.2 All-atom MD simulations of H1 peptide of colicin U in model lipid bilayers

Although the crystallographic structure of colicin U remains undetermined, its interaction with lipid membranes has been previously explored using black lipid membrane (BLM) techniques [86] and fluorescence techniques by a collaborating laboratory at the Depart-

ment of Microbiology, Faculty of Science, Charles University. Based on these experimental insights, it was hypothesized in collaboration with the laboratory that the CTD of colicin U exhibits pore-forming capabilities. This collaboration aimed to investigate the molecular mechanisms behind the pore-forming activity of individual helices within the CTD of colicin U. The collaborating team provided a homology model of the CTD of colicin U, constructed using the iTasser software [87]. Our initial focus was on the H1 helix of the CTD. Utilizing multiple sequence alignment with Clustal Omega [88, 89], we extracted this peptide from the model, embedded it into a lipid membrane model, and conducted MD simulations. The sequences used for comparison included pore-forming colicins with known crystallographic structures [90], are listed here: colicin A - PDB ID: 1COL [91], colicin B - PDB ID: 1RH1 [92], colicin Ia - PDB ID: 1CII [93], colicin E1 - PDB ID: 2I88 [94], colicin N - PDB ID: 1A87 [95], colicin S4 - PDB ID: 3FEW [96].

The H1 peptide was synthesized and experimentally evaluated for antimicrobial activity by the collaborating laboratory. I participated in this experimental phase for several months. The investigation revealed that the H1 peptide did not exhibit behavior indicative of a viable candidate for targeted antibiotic treatment, leading to the cancellation of further planned MD simulations within our TFLL model environment.

3.2.1 Preparation of H1 peptides and model lipid membranes for MD simulations

In our published work, we compared the behavior of the H1 peptide from colicin U with those from the CTD of colicin A and Ia, which are frequently studied experimentally. We sourced the structures of these colicins from the Protein Data Bank [97], extracting the relevant H1 helices. For example, from colicin A (PDB ID: 1COL [91]) residues 5-31 were used, and from colicin Ia (PDB ID: 1CII [93]) residues 442–468 were employed. Our homology model for colicin U's H1 included residues 1-27. The H1 amino acid sequences and extracted helical segments of CTD from these colicins are depicted in Figure 3.5. A control synthetic hydrophobic helix, peptide LW21, used in our prior studies [98], had the following amino acid sequence: GLLDSKKWWLLLLLLLALLLLLLLWWKKFSRS [99].

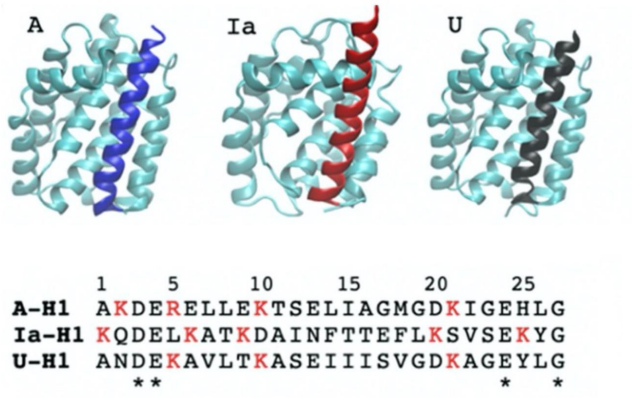

Figure 3.5: CTD structures of colicin A, Ia, and U with highlighted H1 helices and sequences, particularly emphasizing arginine and lysine residues. This image is taken from our publication [99].

We examined the behavior of these three H1 peptides in three model lipid membranes corresponding to mammalian and bacterial cell lipid compositions. The mammalian cell [100] model membrane consisted of 128 POPC lipids (1-palmitoyl-2-oleoyl-sn-glycero-3-phosphatidylcholine), while the gram-negative bacterial [101] models contained 128 lipids of either POPE (1-palmitoyl-2-oleoyl-sn-glycero-3-phosphoethanolamine) or POPG (1-palmitoyl-2-oleoyl-sn-glycero-3-phosphoglycerol). The chosen lipid force field was Slipid, compatible with protein simulations [102, 103]. Each system was solvated with approximately 5 000 water molecules, modeled by the TIP3p water model [104, 105].

Physiological ion concentrations were maintained with K^+ and Cl^- at 0.154 M. K^+ was preferred over Na^+ to avoid interaction artifacts with the POPC membrane [106]. The POPG membrane required neutralization with K^+ counterions due to its negative charge. Additional K^+ ions were added to balance the net charge of peptides that had a higher count of negative versus positive amino acid residues. Ion parameters were adopted from Dang's FF [107].

3.2.2 MD simulations of H1 peptides in model lipid membranes

All MD simulations were performed using GROMACS 2016.4 [108]. The AMBER99SB-ILDN force field was selected for the calculations of excised peptides from the CTD colicins [109].

Peptides were laterally integrated into the membranes with their transmembrane orientation fixed, employing high lateral external pressure based on protocols outlined in paper [110]. Following peptide integration, energy minimization was conducted in 1 000

steps using a steepest descent algorithm [49, 64], succeeded by gradual heating of the systems through short equilibration runs at temperatures of 50 K and 200 K, before commencing NPT ensemble MD simulations at 310 K and 1 bar.

PBC were employed throughout all simulation stages. The motion of individual atoms in the system was calculated using an integration timestep of 2 fs, facilitated by established bond restraint algorithms for bond vibrations. In MD simulations, maintaining a fixed bond length generally provides a more accurate approximation than a harmonic spring, enhancing the simulation's performance [49]. Covalent bonds were constrained using the LINCS algorithm [111, 112], while vibrations in water molecules were managed with the SETTLE algorithm [113].

The systems were regulated at a constant temperature of 310 K and pressure of 1 bar using a Nose-Hoover thermostat [114] and a semi-isotropic Parrinello-Rahman barostat [115]. The thermostat coupling time constant was set to 0.5 ps, and the barostat coupling time constant to 10 ps. Semi-isotropic pressure coupling allows the simulation box to vary uniformly in the x and y dimensions while differing in the z dimension, a configuration typically preferred for membrane simulations [116].

Electrostatic interactions were handled using the particle mesh Ewald (PME) method [117], with a cutoff of 1.4 nm for short-range interactions and 1.6 nm for long-range non-bonding interactions. The PME method calculates infinite electrostatic interactions by dividing them into the sum of short-range and long-range components, with the balance determined by the cutoff value [49].

After initiating the simulation runs, the first 300 ns were allocated for system equilibration. Subsequently, only the last 200 ns of the total 500 ns trajectory were used for analysis. The transition from non-equilibrated to equilibrated system was determined by analyzing the root-mean-square deviation (RMSD) of the peptide structure and calculating peptide-lipid contacts.

4. Results and discussion

This chapter synthesizes the findings from my doctoral research, which have been published across four articles (Publications I - IV). Throughout these publications, my contributions were in the domain of molecular dynamics (MD) simulations, rather than experimental work. Consequently, the results discussed herein are derived solely from these simulations. These attached studies investigated the interactions of potentially new pharmacological agents with lipid environments (multilayers and bilayers), with a specific focus on the lipid film at the surface of the human eye.

4.1 Pharmacologically relevant compounds studied

This dissertation includes research on four types of compounds, each with implications for pharmacological research and lipid interfaces in the context of human eye. Below is a brief overview of these compounds:

- **Latanoprost (LTP)**: LTP, an ester prodrug, undergoes activation to its free acid form within the cornea. Alongside topical prostaglandins, it is commonly the first-line pharmacological treatment for primary glaucoma and ocular hypertension [30]. Typically, it is administered via eye drops that often include BAKs as a preservative.

- **Benzalkonium chloride (BAK) surfactants**: BAK compounds are categorized within the group of quaternary ammonium compounds, which are known for their excellent solubility in water and surface-active properties. BAKs are composed of a mixture of alkylbenzyldimethylammonium chlorides, featuring alkyl chains ranging from C8 to C18. These compounds are widely utilized as preservatives in eye drops that contain active pharmaceutical ingredients, such as LTP.

- **Surfactant protein G (SP-G)**: SP-G belongs to the surfactant proteins (SPs) family, which plays a role in forming a layer of surface-active phospholipids at the fluid-air interface within pulmonary structures. While these proteins are predominantly associated with the lung alveoli, they are also present in various other human body sites, including the ocular surface, where they exhibit immunological proper-

ties. The newly identified SP-G differs subtly from other SPs, distinguished by a unique structure characterized by amphipathic residues.

- **Peptide H1 from the CTD of colicin U**: A potentially novel antimicrobial peptide, capable of disrupting lipid membranes, was derived from the pore-forming CTD of colicin U, which comprises ten alpha-helices. Several of these helices may play a crucial role in the action mechanism of this pore-forming colicin. Colicin U is synthesized by *Shigella boydii* [42, 44] and functions as a competitive agent in both intraspecific and interspecific bacterial interactions.

4.2 Publication I - Latanoprost incorporates in the tear film lipid layer: An experimental and computational model study

This chapter presents results from a basic CG MD simulation study describing the interaction of LTP with TFLL. These results are available in Publication I.

4.2.1 Latanoprost aggregation dynamics in aqueous environments

Our investigation into latanoprost's behavior in aqueous solutions utilized CG MD simulations to explore how LTP aggregates in an environment simulating physiological conditions. In these simulations, we initially positioned 50 LTP molecules in a simulated aqueous box containing approximately 20 000 water molecules (approximately 5 000 MARTINI water beads). This high concentration setup, approximately 25 mmol, significantly exceeds typical concentrations found in ophthalmic products, facilitating the observation of molecular interactions over a microsecond timescale.

During the simulation, initially dispersed LTP molecules began forming smaller clusters within nanoseconds, progressively coalescing into a single, large aggregate over the course of the simulation. This formation process, culminating in a stable large aggregate within 1 µs, illustrates the inherent tendency of LTP to nucleate in water despite its low solubility. The dynamic behavior of the LTP clusters, maintaining liquid-like properties, was captured in our simulation snapshots (Figure 4.1).

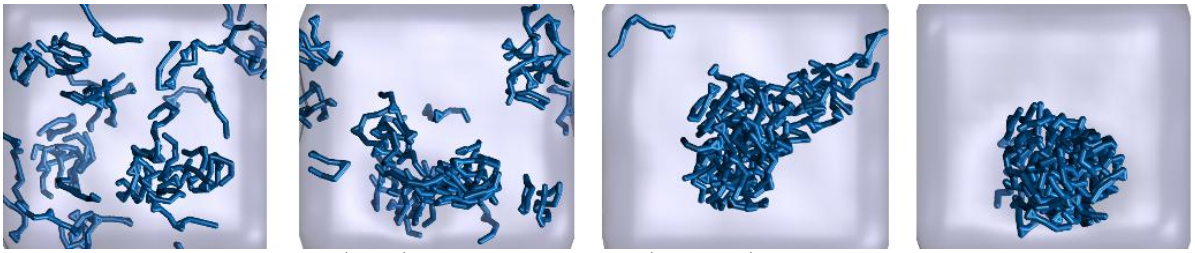

Figure 4.1: LTP molecules (blue) in the water bulk (ice blue) during the 1 μs simulation. Images are taken from our publication [118].

Quantitative analysis through contact metrics between LTP molecules and water (Figure 4.2) demonstrated a rapid decrease in their interactions as LTP aggregated, effectively minimizing energetically unfavorable contacts with the aqueous medium. Further structural analysis using radial distribution functions (shown in the paper) revealed that the core of the LTP nanodrop predominantly consists of LTP's polar moieties, while hydrophobic groups are oriented closer to the aqueous interface. This behavior contradicts typical hydrophobic/hydrophilic interactions due to the aggregate's small size.

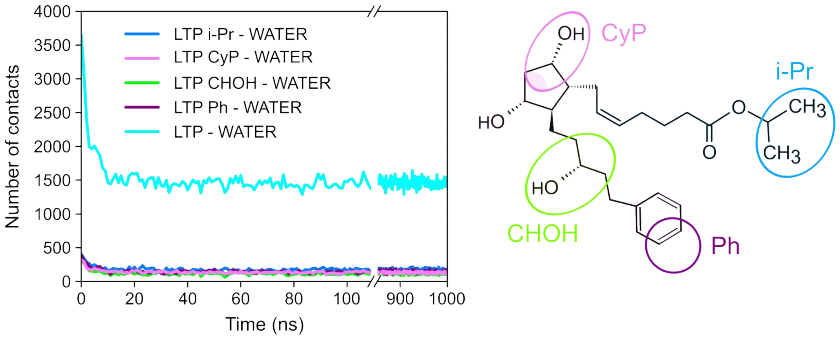

Figure 4.2: Left - Analysis of the number of contacts between LTP and water, and between different parts of LTP and water. Right - Chemical structure of LTP and its MARTINI model. Images are taken from our publication [118].

4.2.2 Behavior of LTP at the water-air interface

Subsequently, we extended our simulations to examine LTP's behavior at the water-air interface, providing a control scenario that contrasts with our TFLL models. By elongating the simulation box along the z-coordinate to create a water-vacuum interface, we tracked the migration of the pre-formed LTP aggregate toward the interface (Figure 4.3). The LTP aggregate swiftly moved to the interface within the first 20 nanoseconds and maintained its position there for the duration of the 1 μs simulation. This migration did not result in any film formation or specific molecular orientation within the aggregate, confirming LTP's lack of surface activity as indicated by experimental data.

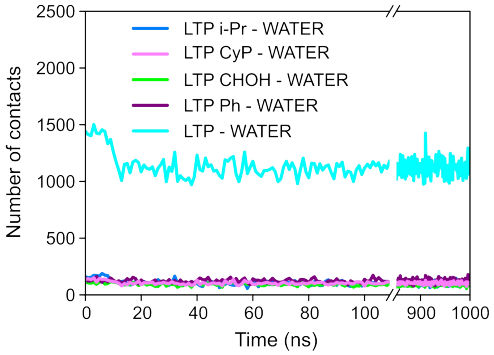

Figure 4.3: Analysis of the number of contacts between LTP and water, and between different parts of LTP and water at the water-air interface. Image is taken from our publication [118].

To verify this behavior of LTP at the interface, further simulations were carried out where the z-coordinate was extended in a box with LTP in a non-aggregated form, randomly distributed among water molecules. Snapshots from this simulation (Figure 4.4) demonstrate that a stable aggregate forms and positions itself at the water-air interface.

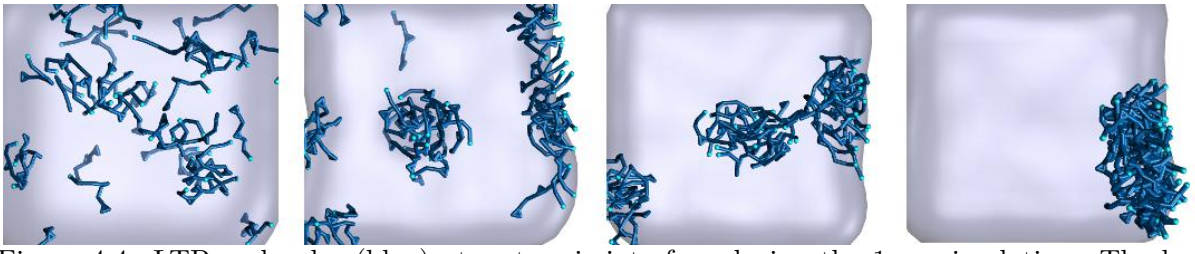

Figure 4.4: LTP molecules (blue) at water-air interface during the 1 μs simulation. The last image in the sequence is taken from our publication [118].

Notably, LTP's affinity for the interface, without forming a structured film, aligns with its observed behavior in practical applications, such as its adsorption to container walls in ophthalmic preparations. These findings highlight the intrinsic hydrophobic interactions driving LTP aggregation and provide insight into the specific chemical groups within LTP that facilitate these interactions.

4.2.3 Interaction dynamics of LTP with TFLL

In our simulations, an aggregate of 50 LTP molecules from previous CG MD simulations in the water cube, initially positioned in the TFLL aqueous subphase, spontaneously migrated and integrated into the lipid film over the course of a 5 μs MD simulation (Figure 4.5).

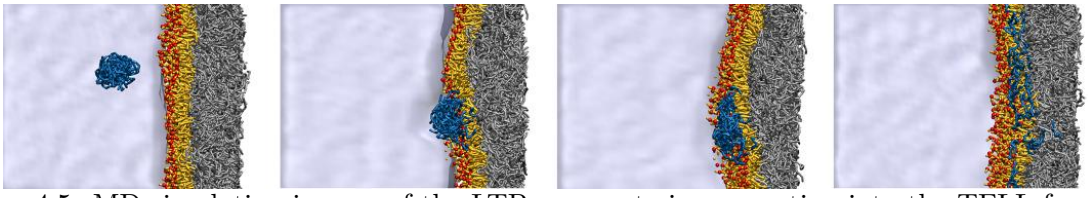

Figure 4.5: MD simulation images of the LTP aggregate incorporating into the TFLL from the aqueous phase during the 5 μs simulation. Color coding: LTP aggregate - blue, PL heads - red, PL tails - yellow, BO and CE - gray, water - gray continuous phase. Images are taken from our publication [118].

The initial engagement of LTP with the lipid layer occurred around 60 ns, marked by significant interactions primarily with the polar lipids. This interaction led to a restructuring phase where LTP, while losing water molecules, increasingly engaged with polar lipids, as evidenced by detailed contact analysis (Figure 4.6, left side). Following engagement, LTP exhibited a protracted period of stabilizing its interactions with polar lipids, culminating in stable incorporation into the polar lipid layer. This integration was characterized by LTP adopting a bent conformation at the water-lipid interface, facilitating interactions predominantly with the heads of polar lipids and, to a lesser extent, their tails. Notably, the dihydroxycyclopentyl (CyP) moiety of LTP displayed distinct behavior by engaging more with non-polar lipids, highlighting the nuanced interaction dynamics of LTP within the TFLL (Figure 4.6). The incorporation of LTP into the TFLL resulted in a slight increase in the interfacial packing and induced minor undulations in the polar lipid layer. These changes were relatively minor due to the low molar ratio of LTP to polar lipids (around 7 %), yet they were consistent with an experimentally observed increase in the lateral pressure of lipid films containing LTP.

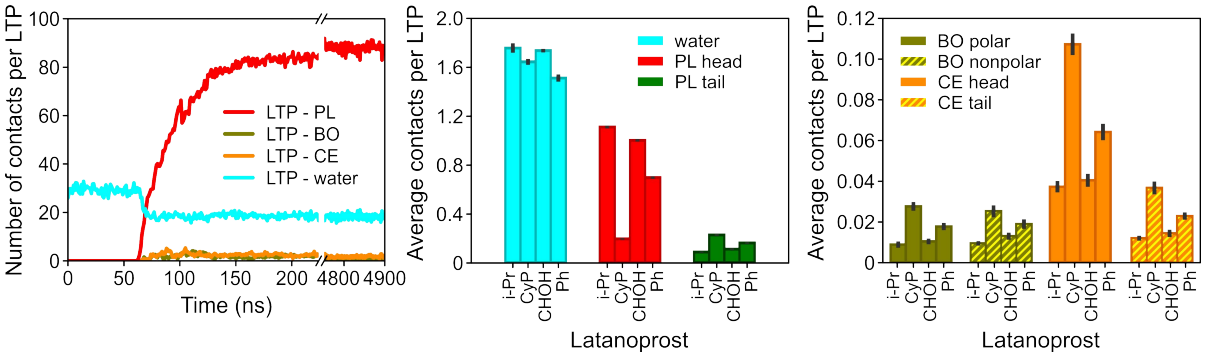

Figure 4.6: Contact analysis of LTP in TFLL. Images are taken from our publication [118].

Additional simulations, in which lateral pressure was reduced by decreasing the polar lipid concentration of the TFLL, showed diminished undulation, underscoring the impact of LTP on the structural integrity of the TFLL. No other qualitative differences were observed, as evidenced by the analysis of density profiles for LTP in TFLL (Figure 4.7).

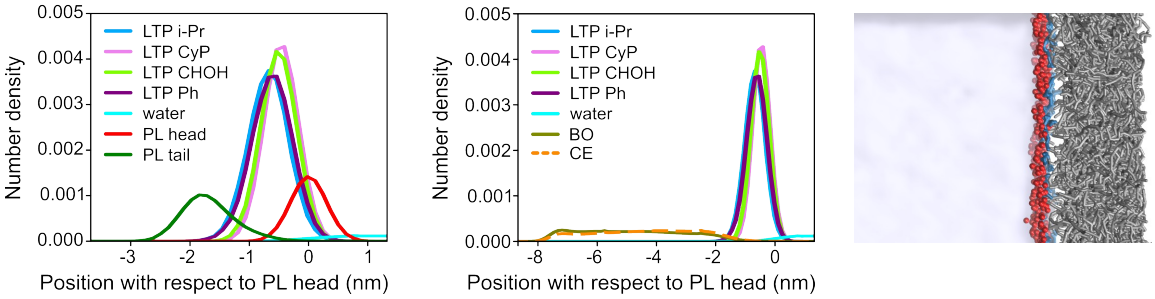

Figure 4.7: Number density analysis of LTP in TFLL: for polar lipids (first figure), for non-polar lipids (second figure). These figures are adapted from our publication [118]. The third image shows a 1.6μs CG MD snapshot of LTP molecules (blue) in a system with reduced polar lipid concentration in TFLL. For better visualization of LTP distribution in the polar layer of TFLL, the acyl chains of POPC are hidden, and only the PL heads (red) are shown. The gray color represents BO and CE.

Further explorations involved control simulations where the LTP aggregate was initially positioned in a vacuum phase above the TFLL, leading to its dissolution predominantly in the non-polar layer before migrating to the polar layer. This process, during which LTP diffused into the polar layer without achieving a fully equilibrated conformation, extended over 12 μs (Figure 4.8). These findings suggest that interactions between LTP and non-polar lipids are preferable and abundant, albeit not leading to complete equilibrium within the simulation time.

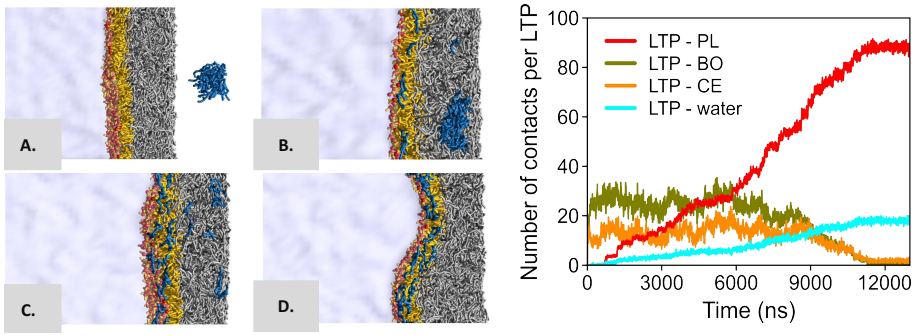

Figure 4.8: MD simulation snapshots of the LTP aggregate incorporating into the TFLL from the water-air interface during the 12 μs simulation (A.-D.) and number of contacts analysis. Color coding: LTP aggregate - blue, PL heads - red, PL tails - yellow, BO and CE - gray, water - gray continuous phase. Images are taken from the SI of our publication [118].

4.2.4 Experimental validation

To empirically validate the MD simulations and further understand the behavior of LTP within the TFLL, a series of experimental studies were conducted in our laboratory using Langmuir isotherms approach. This method effectively measured the changes in lateral pressure at the water-air interface, crucial for assessing the impact of LTP on the structural dynamics of lipid films under varying conditions of lateral packing.

Initially, the experiments focused on films composed solely of polar lipids. Later, the model was extended to include the non-polar components. The addition of LTP dissolved in chloroform to the lipid-covered interface allowed for direct observation of the drug's distribution and integration into the lipid monolayer. As the solvent evaporated, LTP was noted to increase the surface pressure, indicating its incorporation into the polar lipids monolayer. This behavior was quantified through subsequent compression cycles, which showed that LTP could reintegrate into the lipid layer after being squeezed out, suggesting a dynamic equilibrium within the layer. By examining the effects of LTP at different initial surface pressures, we established a correlation between the simulation predictions and the experimental behavior of LTP, particularly regarding its ability to increase lateral pressure and accumulate within the TFLL.

4.2.5 Discussion

Summary of findings:

This study systematically explored the interactions of the anti-glaucoma drug LTP with the TFLL using a combination of in vitro biomimetic models and in silico MD simulations. Our approach has elucidated how LTP integrates into and affects the structural dynamics of the TFLL, providing valuable insights into its potential therapeutic implications.

The experiments demonstrated that LTP could significantly alter the molecular packing within the TFLL, with the layer capable of incorporating LTP up to a molar ratio of 9:1 relative to polar lipids. Such a high accommodation capacity suggests that the TFLL could act as an effective reservoir for sustained LTP release, which is crucial for prolonged therapeutic action in treating glaucoma.

Simultaneously, MD simulations provided a molecular-level view of how LTP aggregates in the aqueous phase and interacts with the lipid layer. Notably, LTP was observed to form micelle-like aggregates in the aqueous environment, orienting its molecules towards water, contrasting with its behavior at the pure water-air interface where it formed a more cohesive aggregate. When integrated into the TFLL model, LTP localized within the hydrated region of the polar heads, indicating a preference for this environment over the non-polar lipid regions. This dissolution and stable integration within the polar heads underscore LTP's potential for immediate and sustained interaction with the TFLL upon

administration.

Implications for clinical practice and drug delivery:

The findings have direct implications for clinical practice, especially considering that LTP is commonly administered with other components like BAKs, enhancing its solubility. The post-instillation dynamics, influenced by factors like blinking, further complicate the drug's interaction with the TF. However, our study suggests that LTP maintains substantial and prolonged contact with the TFLL, supporting its therapeutic efficacy over extended periods.

Given the dynamic and non-equilibrium nature of the TF post-eye drop administration, traditional methods of quantifying drug release via equilibrium-based metrics may not provide accurate insights. Thus, developing in vitro methods that can more directly account for these dynamics is essential for advancing our understanding and optimization of ocular drug delivery systems.

Building on these insights, there is a promising avenue for the development of drug delivery systems that leverage the interaction of LTP with non-polar lipids. Formulations such as oil-in-water emulsions could be particularly effective, potentially enhancing the localized concentration of LTP within the lipid component of the TF. Such strategies could optimize the therapeutic profiles of anti-glaucoma medications, improving patient outcomes by stabilizing drug levels within the ocular environment.

4.3 Publication II - Influence of BAKs on tear film lipid layer: In vitro and in silico models

This chapter details the interaction mechanisms of BAK compounds with the TFLL, as part of Publication II. It also includes additional data not directly featured in this publication.

The investigation focuses on the behavior of BAK compounds within both aqueous and lipid environments of the TF, subsequent to topical application via eye drops. The study initially examines the behavior of BAKs in aqueous solution at two concentrations: low (approximately 0.04 M) and high (approximately 0.2 M). These concentrations were

selected to mimic post-application dilution and initial application conditions, respectively. Both are above the critical micellar concentration (0.15 mM) [119], facilitating the CG MD equilibration process. Further, the study explores BAK activity at the water-air interface to assess their surface activity, providing a dual perspective on their behavior in different phases of the TF.

The TFLL model's composition (see Methodology section 3.1.1 for details) mimics the pressure properties of POPC in bilayers as well as the dense liquid-condensed phase of the POPC monolayer, set to an APPL of 0.67 nm^2. Through CG MD simulations, we observed the behaviors of BAKs post-application, analyzed at both low (around 0.02 M) and high (around 0.15 M) concentrations. The high concentration corresponds to the immediate post-application scenario, while the low concentration simulates the dilution during the natural TF turnover and blinking processes.

4.3.1 BAKs behavior in aqueous environments

Low concentration: CG MD simulations demonstrate that, at low concentrations, BAK compounds predominantly exist in monomeric or dimeric forms within a cubic water environment. A longer time scale is needed to form a micelle-like aggregate compared to high concentrations of BAKs. For BAK8, aggregation is minimal at this dilution level.

High concentration: Conversely, at high concentrations, BAK compounds exhibit rapid aggregation, forming elongated micellar structures. This increased tendency to cluster was observed during CG MD simulations and is detailed in Figure 4.9. These large micelle-like aggregates consists of several smaller subunits, highlighting the compounds' propensity for more substantial aggregation under conditions mimicking immediate post-application of eye drops.

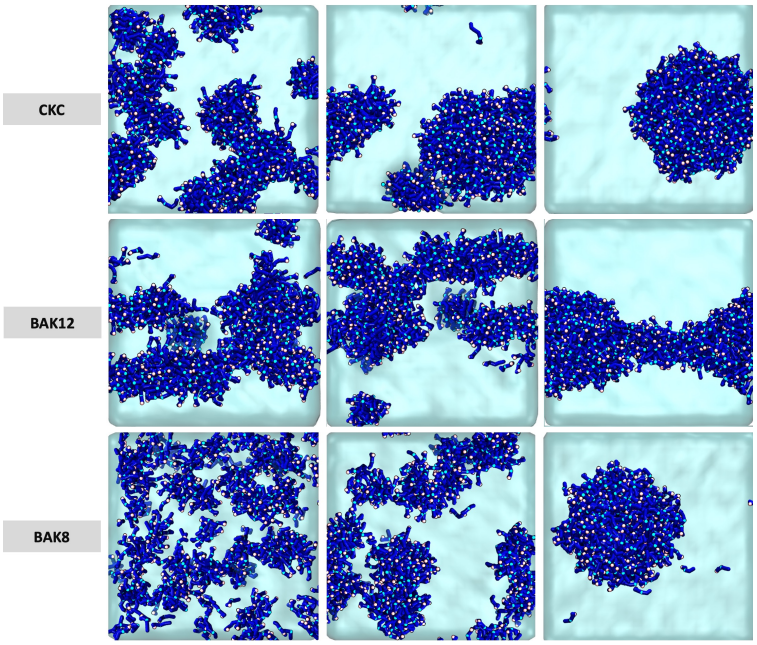

Figure 4.9: Formation of elongated micellar aggregates by BAKs at high concentration in the aqueous environment during a 1 μs CG MD simulation. Periodic boundary conditions are used in cubic MD boxes. Color coding: BAKs - dark blue, polar heads of BAKs - light blue and pink, water - turquoise. Similar visualizations were used in our publication [33] for CKC.

4.3.2 BAKs behavior at the water-air interface

Low concentration: At the water-air interface, BAKs at low concentrations migrate towards the interface, forming a film. This film formation, predominantly by CKC and BAK12, is due to their longer aliphatic chains compared to BAK8, which forms a less consistent surface film due to its shorter chain length.

High concentration: At higher concentrations, BAKs form micellar structures that also migrate to the interface, subsequently creating a more consistent film. This supports our hypothesis regarding the inherent surface activity of BAKs, allowing them to form a film at the interface or aggregate to minimize exposure to the aqueous environment when film formation is not possible. The process and resulting film formation at high concentrations are depicted in Figure 4.10.

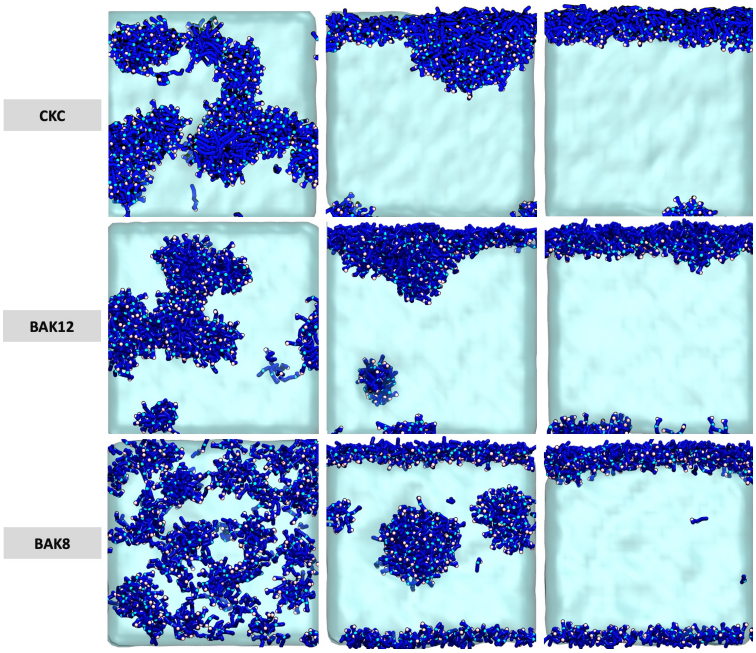

Figure 4.10: Micellar structures and film formation by BAKs at high concentration at the water-air interface during a 1 μs CG MD simulation. Air-water interfaces are formed at the top and bottom of each MD box. Color coding: BAKs - dark blue, polar heads of BAKs - light blue and pink, water - turquoise. Similar visualizations were used in our publication [33] for CKC.

To verify this behavior and reduce the interaction of non-aggregated BAKs with two air-water surfaces, we also ran control simulations where already aggregated forms of BAKs from previous simulations were chosen for the starting conditions (Figure 4.11).

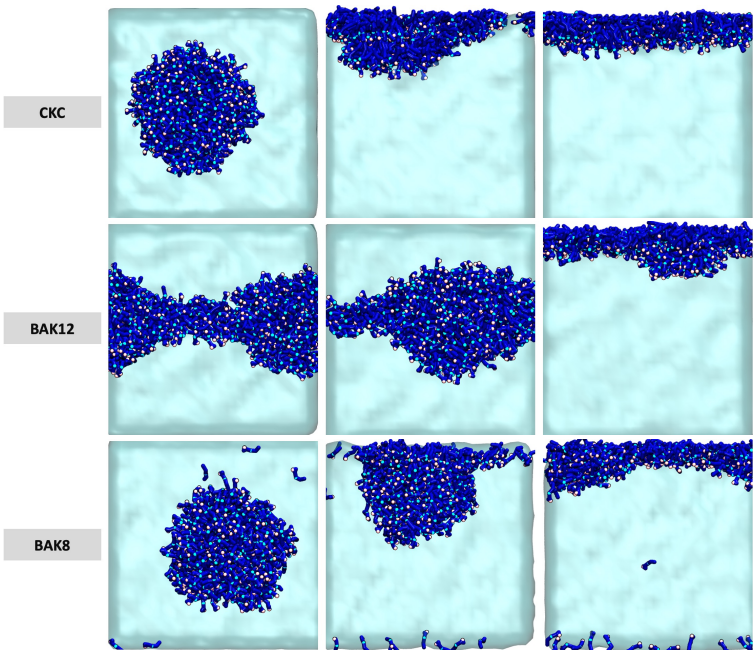

Figure 4.11: Control MD simulations: Film formation by BAKs at high concentration at the water-air interface during a 1 μs CG MD simulation. In this case, the starting position of BAKs was from an already formed water aggregate. Air-water interfaces are formed at the top and bottom of each MD box. Color coding: BAKs - dark blue, polar heads of BAKs - light blue and pink, water - turquoise.

4.3.3 BAKs interaction with the TFLL Model

Low concentration:

In CG MD simulations, BAK compounds remain stably integrated among the polar POPC lipids in the TFLL throughout the simulation period. Typical snapshots from these simulations, which capture the stable positioning of BAKs among POPC lipids, are shown in Figure 4.12. This figure illustrates typical snapshots of this interaction, emphasizing the orientation of the surfactant molecules: polar heads facing the aqueous phase and non-polar tails directed towards the non-polar layer of TFLL.

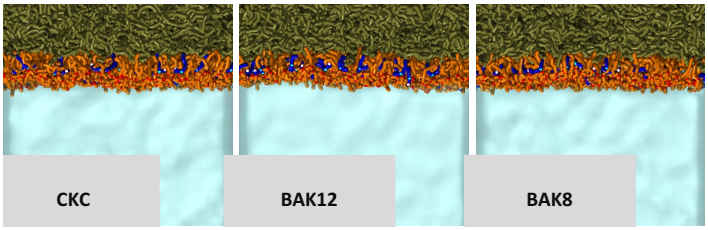

Figure 4.12: BAKs at low concentration within the TFLL. These are CG MD snapshots corresponding to a 1.6 μs simulation time. Color coding: PL heads - red, PL tails - orange, BO and CE - olive, BAKs - dark blue, polar heads of BAKs - light blue and pink, water - turquoise. Similar visualizations were also used in our publication [33] for CKC.

The precise quantification of these orientations is detailed in Figure 4.13, where the density profiles of BAKs and TFLL are compared. This analysis revealed no significant structural changes within the TFLL at low CKC concentrations.

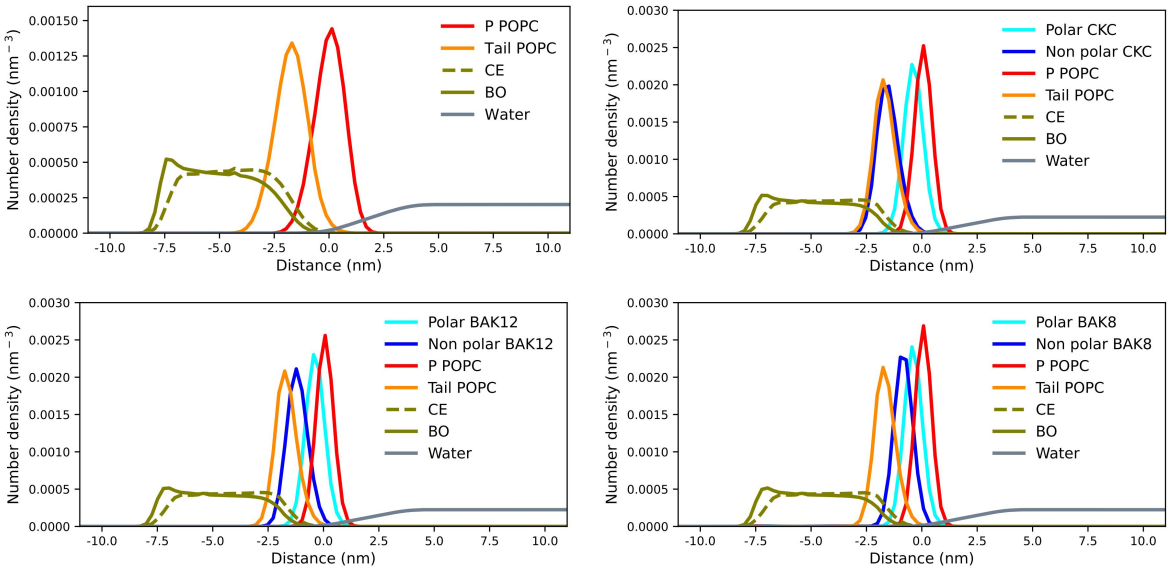

Figure 4.13: Density profile analysis: The upper left figure describes the pure TFLL's density profile, whereas the others show the density profile of BAKs at low concentration. Part of the images for this analysis was sourced from our publication [33].

However, a different behavior was noted for shorter-chain BAKs (BAK8 and BAK12),

which exhibited less ordered alignments within the POPC polar component of TFLL. This difference in molecular behavior is further quantified through tilt angle analysis, shown in Figure 4.14, which illustrates that CKC molecules, with their longer chains, align parallel to the chains of POPC.

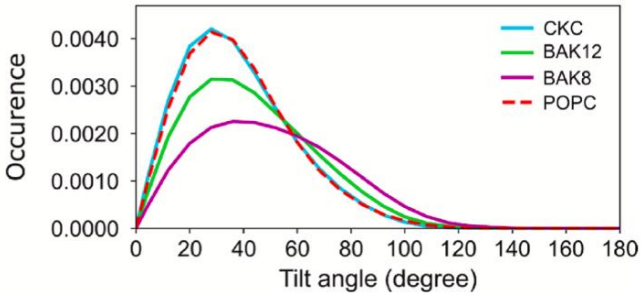

Figure 4.14: Tilt angle analysis of BAKs in the TFLL. The image for this analysis is taken from our publication [33].

Conversely, BAK12 molecules, possessing shorter chains, display a broader range of tilted orientations. The shortest-chain BAK8 molecules undergo the most frequent orientation changes. This variance in molecular orientation, previously observed in our other studies [32], aligns with experimental observations and highlights the nuanced behavior of BAKs within the TFLL.

Thus, the molecular orientations significantly influence the TFLL's functionality. Specifically, CKC's long-chains increase lateral pressure, thereby enhancing the barrier properties of the layer and reducing the likelihood of water penetration. In contrast, BAK8, with its shorter chain, exerts less lateral pressure, permitting greater water infiltration into the polar layer of the TFLL, which could lead to the formation of water defects. BAK12, with a chain length intermediate between CKC and BAK8, exhibits transitional behavior, balancing between structure and permeability.

High concentration:

At higher concentration, the behavior of BAKs in the TFLL indicates a significant restructuring of the POPC layer. Figure 4.15 presents snapshots from CG MD simulations illustrating the behavior of BAK aggregates. CG MD simulations reveal the gradual dissolution and integration of BAK aggregates into the polar POPC layer, restructuring it and leading to behavior resembling a collapse of the POPC layer. This process involved also the transport of POPC molecules into the non-polar TF layer along with BAK molecules,

water molecules, and counterions, forming structures resembling elongated inverse micelles within the non-polar phase.

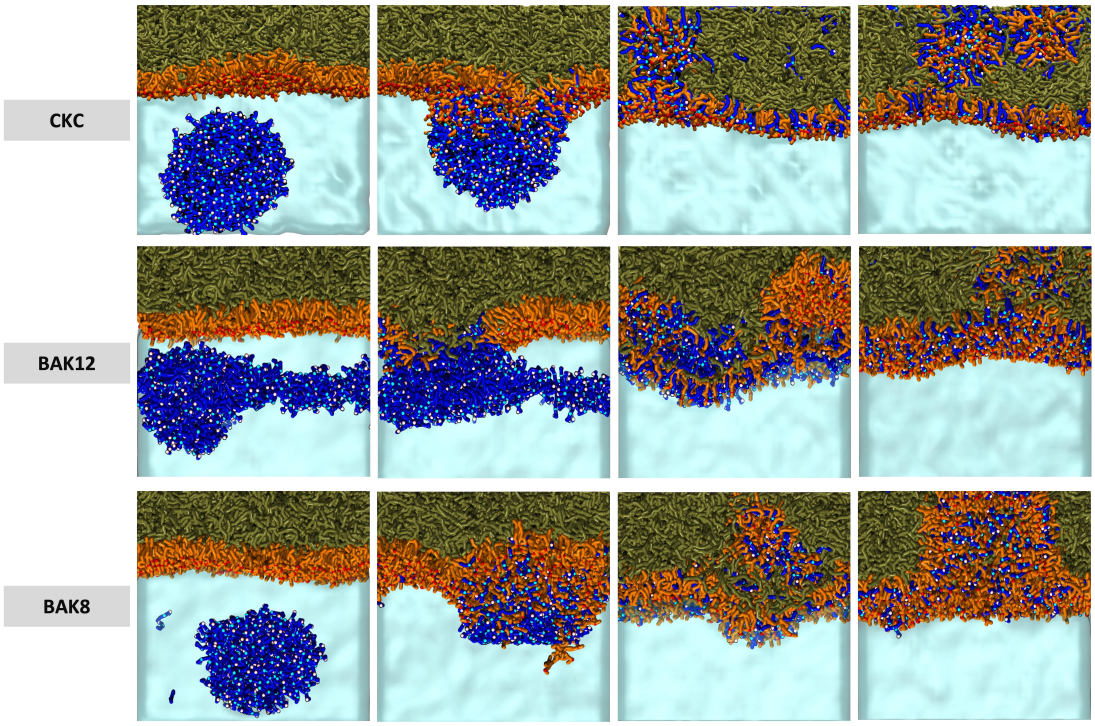

Figure 4.15: CG MD snapshots of BAKs at high concentration in TFLL during 3 μs simulation time. Color coding: PL heads - red, PL tails - orange, BO and CE - olive, BAKs - dark blue, polar heads of BAKs - light blue and pink, water - turquoise. Similar visualizations were used in our publication [33] for CKC.

This significant reorganization, depicted in Figure 4.16 through density profile analysis, facilitates the transport of active drug components within the TFLL, which could be critical for the efficacy of topical eye treatments.

Further, we observed that BAKs migrating through the polar POPC component into the non-polar component reached the lipid-air interface over time and formed a film on this surface. This behavior indicates a dynamic rearrangement and accumulation of clusters of BAKs, POPC, water, and counterions in the non-polar layer of the TFLL.

Such observations underscore the potential for drug component accumulation in the non-polar layer of the TFLL, which is relatively stable over time compared to the aqueous phase [120]. This stability may play a crucial role in the sustained delivery and efficacy of drugs applied to the surface of the human eye.

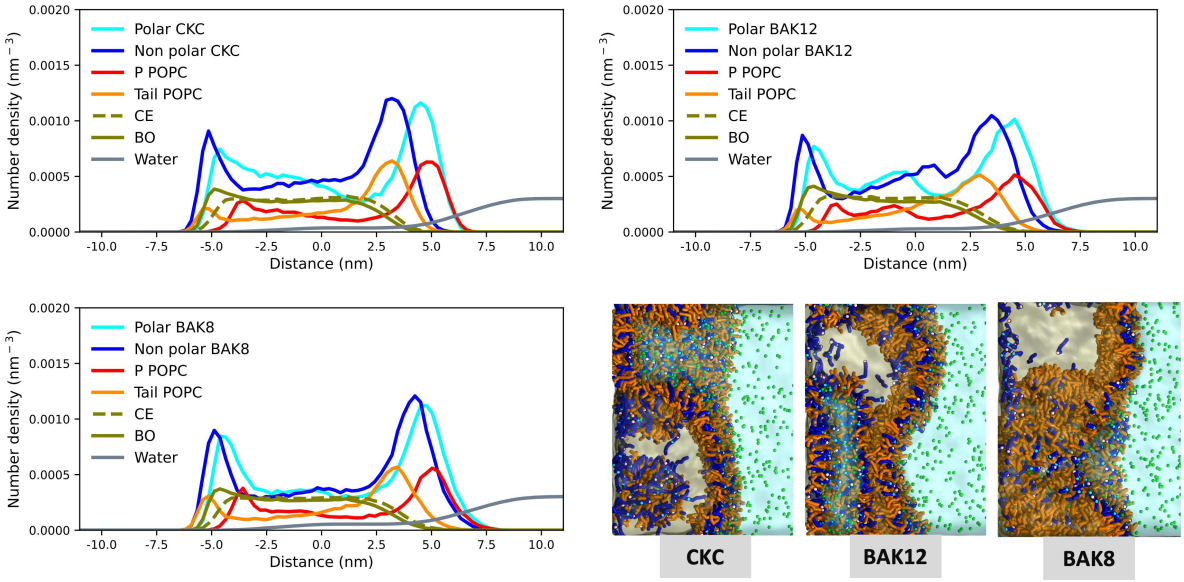

Figure 4.16: Density profile analysis of BAKs at high concentration within the TFLL. VMD snapshots depict the BAK aggregates during the simulation, with the tails of POPC shown in orange, BAKs in dark blue, BO and CE in transparent olive, water in turquoise, polar heads of BAKs in light blue and pink, and Cl^- counterions in green. The density profile of CKC is adapted from our publication [33]; others have been added.

4.3.4 Experimental validation

The CG MD simulation results were corroborated by experimental measurements using the Langmuir trough technique to assess the effects of BAKs on lateral pressure and molecular packing in a TFLL experimental model. This method provided macroscopic insights into the structural dynamics of the TFLL under the influence of BAKs. Surface pressure-molecular area isotherms were recorded for both control (without BAKs) and test (with BAKs) systems. Additionally, widefield fluorescence imaging and generalized polarization measurements were employed to visualize and analyze the lipid arrangement within the TFLL in the presence of various BAK compounds. These measurements offer direct experimental evidence aligning with our simulation results, affirming the impact of BAKs on the TFLL's structure and function.

4.3.5 Discussion

Summary of findings:

The interaction of BAKs with the TFLL model demonstrates a significant influence based on the surfactant's chain length. Long-chain BAKs, such as CKC, enhance lateral packing

and order within the TFLL, potentially optimizing the barrier properties of the lipid layer. In contrast, shorter-chain BAKs, like BAK8, introduce more flexibility and disorder, potentially compromising the structural integrity and increasing susceptibility to water infiltration.

Implications for drug delivery:

Our findings suggest a dual role for BAKs in topical eye treatments. Immediately post-application, high concentrations of BAKs facilitate the formation of micelle-like aggregates that interact with the polar layer, potentially aiding in the transport of active drug components. Over time, as BAK concentrations diminish due to natural ocular defense mechanisms and dilution, the surfactants integrate into the polar layer of the TFLL, influencing its function according to their molecular structure.

The long-term usage of BAK-containing eye drops could have varying effects depending on the BAK composition. While long-chain BAKs may enhance the structural stability of the TFLL, short-chain variants could disrupt it, making their use less desirable in prolonged treatments. This insight is crucial for developing safer and more effective eye drop formulations that leverage the unique properties of BAKs.

4.4 Publication III - The potential role of SP-G as surface tension regulator in tear film: From molecular simulations to experimental observations

This chapter presents the results from the study of the interaction of the SP-G protein with TFLL, which are part of Publication III.

In MD simulations, the interaction dynamics of SP-G with the TFLL were analyzed across models with varying lipid packing densities. Three distinct APPL values were examined: approximately 0.7 nm^2, 1.0 nm^2, and 1.3 nm^2. In each model, SP-G was positioned about 2 nm from the water-lipid interface within the aqueous subphase.

4.4.1 SP-G adsorption to the TFLL

In systems with tighter lipid packing (APPL = 0.7 nm^2 and 1.0 nm^2), SP-G did not adsorb to the lipid film throughout the 1 μs simulation. Conversely, in the system with the least dense packing (APPL = 1.3 nm^2), SP-G rapidly adsorbed to the interface between water and the polar headgroups of POPC, approximately at 250 nanoseconds. Following this adsorption, SP-G began to integrate into the lipid film, achieving a stable orientation that persisted for the remainder of the simulation time. TFLL compression and SP-G behavior are captured in snapshots from the simulation (Figure 4.17).

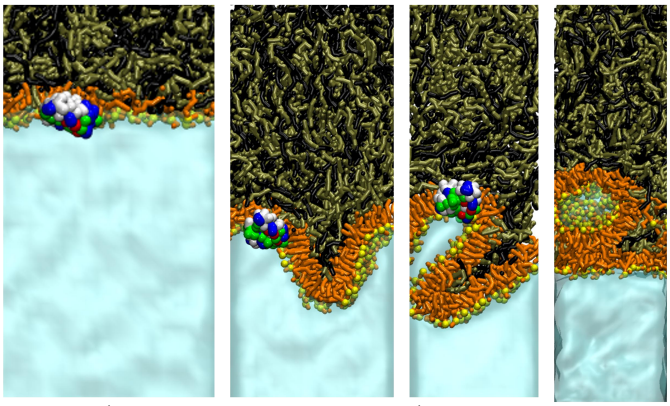

Figure 4.17: MD snapshots (first three from the left) of lateral compression of TFLL in the presence of SP-G during CG MD simulation. The last image shows the collapse of the TFLL without the presence of SP-G. Color coding: BO - black, CE - olive, POPC - orange, PO_4 of POPC - yellow, water - turquoise, SP-G protein - ResType.

4.4.2 Protein-lipid interaction analysis

Further investigation into the interactions between SP-G and the TFLL showed distinct patterns of behavior for the different residue types of the protein. Polar, basic, and acidic residues predominantly interacted with water and the polar components of the TFLL. Meanwhile, hydrophobic residues penetrated deeper, engaging primarily with non-polar components of the TFLL, such as CE lipids. This behavior is described by analyzing the number of contacts for individual SP-G amino acids, as shown in Figure 4.18. The adsorption of SP-G not only altered the structural configuration of the POPC layer but also facilitated the formation of a pore within it, which was occupied by both the protein itself and water molecules. These water molecules were drawn into the pore in the TFLL layer due to the influence of the hydrophilic amino acid residues of the protein, as shown in the spatial density profiles analyses available in the publication.

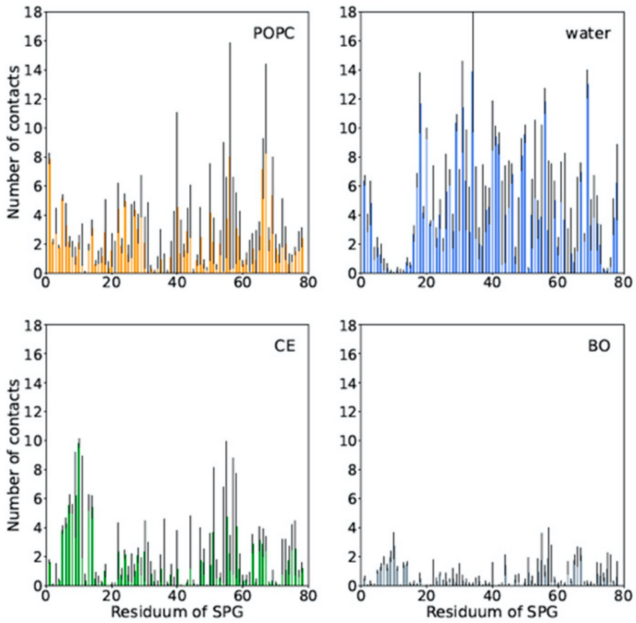

Figure 4.18: Analysis of the number of contacts of individual amino acids of the SP-G protein with POPC, water, CE, and BO. This figure was extracted from our publication [39].

4.4.3 Structural dynamics under lateral compression

Additional simulations assessed the TFLL's structural dynamics when adsorbed SP-G was present, utilizing lateral compression from an APPL of 1.4 nm^2 to 0.3 nm^2 over 200 nanoseconds. This process induced notable structural changes in the TFLL, including the development of undulations in the polar POPC layer, followed by the formation of invaginated structures. Despite these significant alterations, the protein continued to be stably adsorbed to the layer, maintaining the continuity of both the polar and non-polar parts of the TFLL. In contrast, when SP-G was absent, the same simulations showed a collapse of the lipid layer, forming inverse micelle-like structures. This event moved water and POPC from the polar region to the non-polar region of the TFLL (Figure 4.17, right side).

4.4.4 Experimental validation

This subsection provides a short summary of the diverse experimental methods applied to validate the MD findings and to explore the roles of SP-G in the ocular environment performed by our collaborators. These experimental methods provided comprehensive insights into the potential biological roles of SP-G in the ocular surface's health and

disease.

Detection and localization: SP-G mRNA was identified in various tissues of the ocular surface and lacrimal apparatus using PCR, confirming its transcription in these tissues as per Genebank data. Proteins from tear fluid samples were analyzed via Western blot, revealing SP-G bands, corroborated by controls from bronchoalveolar lavage fluid. Immunohistochemistry was employed to localize SP-G in tissues such as the lacrimal and meibomian glands, and corneal and conjunctival epithelium, highlighting its widespread presence across ocular tissues.

Quantitative analysis: The concentration of SP-G in tears and ocular tissues was quantified using ELISA, revealing elevated levels in patients with dry eye disease compared to healthy controls. This suggests a potential protective or compensatory role of SP-G in ocular surface disorders.

Functional assays: The surface activity of SP-G was assessed by measuring the surface tension of tear films using a spinning drop tensiometer, demonstrating that SP-G concentrations influence tear film stability. Additionally, the wound healing scratch assay on corneal epithelial cells indicated that SP-G enhances wound closure, potentially supporting corneal repair processes.

Effect of cortisol: The influence of cortisol on SP-G expression was investigated in human corneal epithelial cells, with findings indicating that cortisol levels significantly impact SP-G mRNA expression, suggesting a stress-responsive element in SP-G regulation.

4.4.5 Discussion

Summary of findings:

Our simulations revealed that SP-G interacts distinctively with the lipid molecules of the TFLL, particularly under varying lipid packing conditions. In less densely packed lipid environments, SP-G demonstrated a propensity to adsorb to the lipid-water interface,

subsequently integrating into the lipid layer. This integration facilitates SP-G's stabilization within the lipid layer, as evidenced by its sustained orientation and interaction with both polar and non-polar lipids. Under conditions of lateral compression, which mimic the dynamic changes in the TF post-blink, SP-G helped maintain the continuity of the lipid layers, preventing the collapse observed in SP-G-absent simulations. This suggests that SP-G not only enhances the mechanical stability of the TF but may also play a protective role against the disruptive effects of blinking and shear stress. Interactions between SP-G and lipid components of TFLL, such as POPC and CE, underscore its ability to interact with both polar and non-polar molecules. These interactions likely contribute to SP-G's capability to modulate surface tension and facilitate wound healing, as indicated by associated experimental studies. The hydration dynamics observed around the hydrophilic residues of SP-G further suggest its role in maintaining hydration.

Broader implications:

While the simulations provide a foundation for understanding SP-G's functional mechanisms at the molecular level, further studies are essential to fully delineate its roles. This is particularly pertinent in the context of dry eye conditions, where SP-G's interaction with tear film lipids could influence treatment strategies for enhancing tear film stability and addressing ocular surface disorders.

4.5 Publication IV - H1 helix of colicin U causes phospholipid membrane permeation

This chapter presents the results, published in Publication IV, from all-atom MD simulations exploring the behavior of H1 peptides, derived from colicin's CTD, within various phospholipid environments. Our work focused on evaluating the potential of the H1 peptide to act as a new antibiotic. In this study, we examined its interaction with lipid bilayers. If the H1 peptide exhibited promising behavior in membranes, we planned to extend the study to its interaction with our TFLL model in a subsequent publication, to assess its potential for the treatment of bacterial colonization of the ocular surface.

H1 peptides derived from three different species of pore-forming colicins were incorpo-

rated into lipid membranes composed of POPC, POPE, and POPG, which are representative of model mammalian plasma membranes and the model inner plasma membranes of gram-negative bacteria, respectively. These peptides were initially positioned in a transmembrane orientation and maintained stable incorporation throughout the 500 ns simulation period. The spontaneous integration of peptides into the hydrophobic core of the lipid bilayer was not observed within the 500 ns timeframe, likely due to the need to overcome substantial energy barriers and requiring extended simulation durations. Although other initial peptide positions relative to the membrane were explored, the H1 peptides generally exhibited less stability and tended to lose their secondary structure during the simulations.

4.5.1 Structural dynamics and water penetration

Snapshots of 500 ns MD simulations of transmembrane-localized H1 peptides within the membrane are depicted in Figure 4.19. These visualizations highlight the impact of H1 peptides on membrane integrity, illustrating disruptions in membrane function and the penetration of water molecules into the lipid bilayer. Maintaining their helical secondary structure throughout the duration of the simulation is evident from the RMSD analysis and the helicity analysis available in the SI of this publication. However, minor restructuring, which is potentially functionally significant, was observed. Structural kink positions were identified around highly hydrophilic residues such as lysine and arginine or residues such as serine and glycine, which contributed to a stable and distinct orientation of the helical segments within the membranes. This observation that the H1 α-helices displayed a tilt relative to the membrane normal is evidenced by the tilt angle analysis available in the SI of this publication.

As illustrated in Figure 4.19, the presence of these H1 peptides in the membranes led to structural reconfigurations across all studied membranes, characterized by the penetration of water molecules into the lipid headgroup region and the subsequent formation of defects. Water penetration was noted within the core of the hydrophobic membrane near the transmembrane peptides as well. In certain instances (H1 of Ia colicin and H1 of colicin U in the POPG bilayer), this led to the formation of stable pores, where water passage was observed. Water molecules in the polar lipid headgroup region caused

a partial reorientation of lipid heads, leading to the remodeling of the water-lipid interface. Gradually, water molecules penetrated deeper into the interior of the membrane as they followed the reoriented POPC headgroups, leading to the formation of toroidal pores. The penetration of water occurred only on one face of the H1 peptides due to their amphipathic nature (one face being more hydrophobic, the other more hydrophilic), with this asymmetry being especially marked in the H1 peptide from colicin U, and it corresponded with increased water infiltration into the membrane core. Charged arginine and lysine residues were primarily hydrated due to their positioning predominantly on one face of the helices, while other polar residues were less hydrated. These observations are evident from the analysis of density profiles of H1 peptides in membranes (shown in publication).

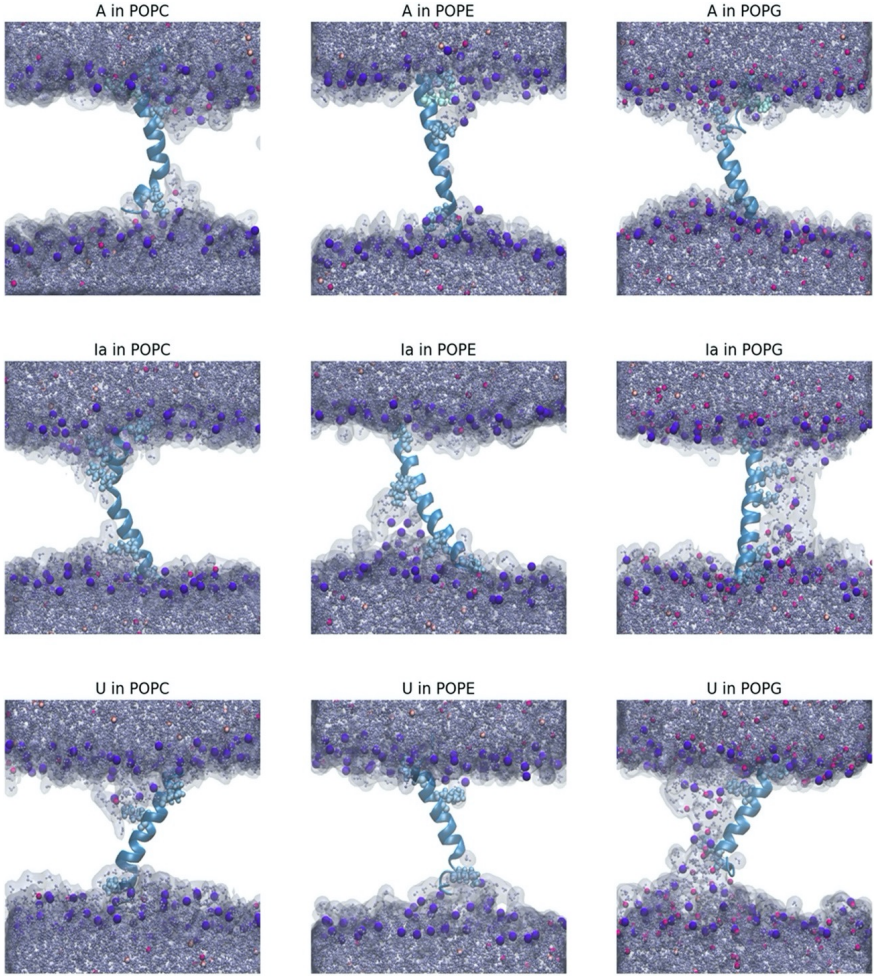

Figure 4.19: MD simulation snapshots of H1 peptides oriented from N-terminus (top) to C-terminus (bottom) at 500 ns, extracted from our publication [99]. In these images, the peptides are colored turquoise, the phosphates of the polar lipid headgroups are visualized in purple, and lipid chains are omitted for clarity. Water molecules are represented in gray, while K^+ ions and Cl^- ions are shown in magenta and pink.

4.5.2 Lipid-peptide interactions

The inclination of lipid headgroups towards the transmembrane-oriented H1 peptide from colicin U was quantitatively analyzed using contact number analysis, as shown in Figure 4.20. In all membranes studied, lipid headgroups tended to cluster around H1 residues, particularly in the POPG membrane where pore formation occurred. This behavior contrasts with our control hydrophobic transmembrane-oriented LW21 peptide with helical secondary structure, where lipid headgroups did not exhibit similar proximity. Transmembrane segments of H1 peptides displayed significantly fewer contacts between peptide and lipid tails during the equilibrated simulations compared to those observed with hydrophobic LW21.

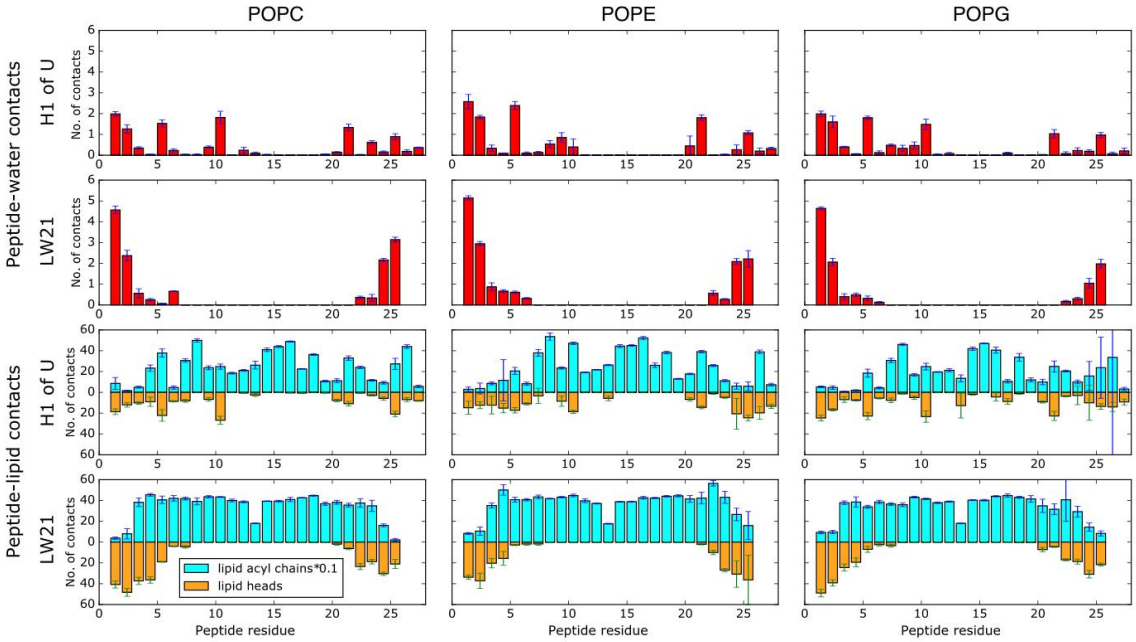

Figure 4.20: Analysis of the number of contacts between water (or lipids) and individual residues of the H1 peptide (derived from the CTD of colicin U) and the control hydrophobic helical LW21 peptide in three model lipid bilayers - POPC, POPE, and POPG. This figure is extracted from our publication [99].

4.5.3 Experimental validation

To validate the findings from MD simulations, several experimental methods were employed, focusing on the interaction between synthetic H1 peptides of CTD of colicin U and model lipid systems.

Liposome leakage assays: We conducted collaborative studies using liposome leakage assays to explore the interaction between synthetic H1 peptides and DOPG liposomes. These assays quantitatively demonstrated that increasing concentrations of H1 peptide lead to enhanced lysis of DOPG liposomes, indicating the peptide's ability to disrupt the membrane structure effectively.

Co-sedimentation assays: To further understand the binding efficiency of the H1 peptide to lipid membranes, we performed co-sedimentation assays. These experiments aimed to quantify the extent of peptide binding to DOPG liposomal membranes. After adding 10 µM of H1 peptide of colicin U to DOPG liposomes, we observed that only about 2.5 % of the H1 peptide was bound to the DOPG. This low binding efficiency correlated with the observed membrane disruption, where even a small amount of bound H1 peptide induced liposomal leakage.

Fluorescence spectroscopy: Fluorescence spectroscopy was employed to detect the binding of H1 peptides to liposomes. The binding efficiency was compared to melittin, a well-known amphipathic peptide used as a positive control, which showed significantly higher membrane binding under similar conditions. Using tryptophan fluorescence for melittin and tyrosine fluorescence for H1 peptides, we were able to determine the binding efficiency of these peptides to the membranes.

Estimation of pore stoichiometry: To estimate the cooperativity of H1 peptide action on liposomal membranes, we analyzed the initial lysis rate as a function of peptide concentration in a double-logarithmic plot. The results suggested significantly low cooperativity, indicating that only small H1 peptide clusters or H1 peptide monomers are necessary to disturb the bilayer.

4.5.4 Discussion

Summary of findings:

The combined insights from MD simulations and experimental assays elucidate the mechanism by which H1 peptides interact with lipid membranes. MD simulations revealed

that the peptides induced significant structural changes within the lipid bilayers. These changes were primarily driven by water molecules infiltrating the lipid headgroup region, potentially leading to toroidal pore formations depending on the specific lipid composition. The helices were found to be tilted with respect to the membrane normal, and kinks were observed at hydrophilic charged lysine and arginine residues, leading to a stable and specific orientation of helical sub-segments in the membranes.

The experimental findings complement these simulation results, particularly through the demonstration of liposome lysis, which aligns with the predicted membrane-disruptive behavior of H1 peptides. This supports the hypothesis that H1 peptides can form pores within lipid membranes, contributing to their potential antimicrobial efficacy.

Therapeutic potential and limitations:

While the study highlights the pore-forming potential of H1 segment peptides from colicin U, the results also caution against their direct application as antimicrobial agents for infections in their current form. The specific interactions and pore formation observed suggest that while effective against model membranes, the functionality and safety of these peptides in therapeutic contexts require further validation and optimization. It is essential to consider their concentration and, most importantly, their selectivity for bacterial membranes over mammalian membranes. For this reason, further investigation of the mechanisms of the effects of this peptide on TFLL was abandoned.

5. Conclusions

The aim of this dissertation was to elucidate the molecular interactions between various ophthalmic drugs or pharmacologically significant compounds and a model of the tear film lipid layer (TFLL) using molecular dynamics (MD) simulations. This research, encompassing studies on latanoprost (LTP) drug, benzalkonium chloride (BAK) compounds, and surfactant protein G (SP-G), revealed several significant insights into the behavior and impact of these compounds on the TFLL. Additionally, the interactions of the H1 peptide, originating from the C-terminal domain of colicin U, were examined with model lipid bilayers composed of POPC, POPE, and POPG.

The findings of this dissertation may have several implications for the development of ophthalmic drug delivery systems. The ability of LTP to integrate into the TFLL underscores the importance of the lipid layer in drug retention and sustained release. This suggests that formulations leveraging lipid interactions could enhance therapeutic efficacy. The dual role of BAKs highlights the need for careful consideration of preservative concentrations to balance drug delivery with TF integrity. Understanding the concentration-dependent effects of BAKs is crucial to mitigate their potential adverse impacts on the TFLL. The potential therapeutic role of SP-G in stabilizing the TFLL offers new avenues for treating ocular surface disorders. SP-G's ability to interact with the lipid layer could be harnessed to develop treatments aimed at improving TF stability and addressing conditions like dry eye syndrome. The pore-forming behavior of the H1 peptide, confirmed through both MD simulations and experiments, suggests its potential as a novel antimicrobial agent. However, the observed interactions and structural disruptions indicate the need for further optimization and validation before therapeutic application, particularly in the delicate environment of the ocular surface.

In conclusion, this dissertation advances our understanding of drug interactions at the ocular surface, providing valuable insights for the development of more effective and safer ophthalmic treatments. The integration of computational simulations with experimental validation offers a robust framework for exploring and optimizing drug delivery systems in the complex environment of the human eye.

References

[1] A. Bunker and T. Róg, "Mechanistic understanding from molecular dynamics simulation in pharmaceutical research 1: Drug delivery," *Frontiers in Molecular Biosciences*, vol. 7, p. 604770, 2020.

[2] M. D. Donovan, "Effect of route of administration and distribution on drug action," in *Modern Pharmaceutics Volume 1*, pp. 173–198, CRC Press, 2009.

[3] S. Doggrell, "Introduction to pharmacology, and routes of drugs administration and absorption," 2017.

[4] A. Seyfoddin, J. Shaw, and R. Al-Kassas, "Solid lipid nanoparticles for ocular drug delivery," *Drug delivery*, vol. 17, no. 7, pp. 467–489, 2010.

[5] A. Puri, "Nanoparticles: Crossing barriers and membrane interactions," *Molecular Membrane Biology*, vol. 27, no. 7, pp. 213–214, 2010.

[6] H. Sasaki, K. Yamamura, K. Nishida, J. Nakamura, and M. Ichikawa, "Delivery of drugs to the eye by topical application," *Progress in Retinal and Eye Research*, vol. 15, no. 2, pp. 583–620, 1996.

[7] I. K. Tadwee, S. Gore, and P. Giradkar, "Advances in topical drug delivery system: A review," *Int. J. of Pharm. Res. & All. Sci*, vol. 1, no. 1, pp. 14–23, 2012.

[8] A. Farkouh, P. Frigo, and M. Czejka, "Systemic side effects of eye drops: a pharmacokinetic perspective," *Clinical ophthalmology*, pp. 2433–2441, 2016.

[9] S. A. Chime and I. V. Onyishi, "Lipid-based drug delivery systems (ldds): Recent advances and applications of lipids in drug delivery," *Afr. J. Pharm. Pharmacol*, vol. 7, no. 48, pp. 3034–3059, 2013.

[10] M. Mofidfar, B. Abdi, S. Ahadian, E. Mostafavi, T. A. Desai, F. Abbasi, Y. Sun, E. E. Manche, C. N. Ta, and C. W. Flowers, "Drug delivery to the anterior segment of the eye: A review of current and future treatment strategies," *International journal of pharmaceutics*, vol. 607, p. 120924, 2021.

[11] G. N. Foulks, "The correlation between the tear film lipid layer and dry eye disease," *Survey of ophthalmology*, vol. 52, no. 4, pp. 369–374, 2007.

[12] R. Montés-Micó, "Role of the tear film in the optical quality of the human eye," *Journal of Cataract & Refractive Surgery*, vol. 33, no. 9, pp. 1631–1635, 2007.

[13] G. Geerling and H. Brewitt, *Surgery for the dry eye: scientific evidence and guidelines for the clinical management of dry eye associated ocular surface disease*, vol. 41. Karger Medical and Scientific Publishers, 2008.

[14] L. Cwiklik, "Tear film lipid layer: A molecular level view," *Biochimica et Biophysica Acta (BBA)-Biomembranes*, vol. 1858, no. 10, pp. 2421–2430, 2016.

[15] S. C. Pflugfelder and M. E. Stern, "Biological functions of tear film," *Experimental eye research*, vol. 197, p. 108115, 2020.

[16] L. Zhou and R. W. Beuerman, "Tear analysis in ocular surface diseases," *Progress in retinal and eye research*, vol. 31, no. 6, pp. 527–550, 2012.

[17] X. Xu, G. Li, and Y. Y. Zuo, "Biophysical properties of tear film lipid layer i. surface tension and surface rheology," *Biophysical Journal*, vol. 121, no. 3, pp. 439–450, 2022.

[18] G. Qin, H. Baidouri, A. Glasser, V. Raghunathan, C. Morris, I. Maltseva, and A. M. McDermott, "Development of an in vitro model to study the biological effects of blinking," *The Ocular Surface*, vol. 16, no. 2, pp. 226–234, 2018.

[19] Á. Esteban, A. Traba, and J. Prieto, "Eyelid movements in health and disease. the supranuclear impairment of the palpebral motility," *Neurophysiologie Clinique/Clinical Neurophysiology*, vol. 34, no. 1, pp. 3–15, 2004.

[20] A. Bron, J. Tiffany, S. Gouveia, N. Yokoi, and L. Voon, "Functional aspects of the tear film lipid layer," *Experimental eye research*, vol. 78, no. 3, pp. 347–360, 2004.

[21] D. H. Szczesna-Iskander, "Post-blink tear film dynamics in healthy and dry eyes during spontaneous blinking," *The Ocular Surface*, vol. 16, no. 1, pp. 93–100, 2018.

[22] N. Yokoi, M. Uchino, Y. Uchino, M. Dogru, M. Kawashima, A. Komuro, Y. Sonomura, H. Kato, K. Tsubota, and S. Kinoshita, "Importance of tear film instability in dry eye disease in office workers using visual display terminals: the osaka study," *American Journal of Ophthalmology*, vol. 159, no. 4, pp. 748–754, 2015.

[23] M. A. Lemp, G. N. Foulks, *et al.*, "The definition and classification of dry eye disease," *Ocul Surf*, vol. 5, no. 2, pp. 75–92, 2007.

[24] E. M. Messmer, "The pathophysiology, diagnosis, and treatment of dry eye disease," *Deutsches Ärzteblatt International*, vol. 112, no. 5, p. 71, 2015.

[25] W. Wang and N. Snider, "Discovery and potential utility of a novel non-invasive ocular delivery platform," *Pharmaceutics*, vol. 15, no. 9, p. 2344, 2023.

[26] F. Fineide, N. Lagali, M. Y. Adil, R. Arita, M. Kolko, J. Vehof, and T. P. Utheim, "Topical glaucoma medications–clinical implications for the ocular surface," *The ocular surface*, vol. 26, pp. 19–49, 2022.

[27] K. Hedman and L.-I. Larsson, "The effect of latanoprost compared with timolol in african-american, asian, caucasian, and mexican open-angle glaucoma or ocular hypertensive patients," *Survey of ophthalmology*, vol. 47, pp. S77–S89, 2002.

[28] A. Alm, "Latanoprost in the treatment of glaucoma," *Clinical ophthalmology*, pp. 1967–1985, 2014.

[29] C. Baudouin, A. Labbé, H. Liang, A. Pauly, and F. Brignole-Baudouin, "Preservatives in eyedrops: the good, the bad and the ugly," *Progress in retinal and eye research*, vol. 29, no. 4, pp. 312–334, 2010.

[30] F. Aptel, R. Choudhry, and I. Stalmans, "Preservative-free versus preserved latanoprost eye drops in patients with open-angle glaucoma or ocular hypertension," *Current Medical Research and Opinion*, vol. 32, no. 8, pp. 1457–1463, 2016.

[31] X. Zhou, X. Zhang, D. Zhou, Y. Zhao, and X. Duan, "A narrative review of ocular surface disease related to anti-glaucomatous medications," *Ophthalmology and Therapy*, vol. 11, no. 5, pp. 1681–1704, 2022.

[32] K. Riedlova, A. Melcrova, A. Olzynska, P. Daull, J.-S. Garrigue, and L. Cwiklik, "Influence of benzalkonium chloride on tear film lipid layer stability: a molecular level view by employing in silico modeling," *Modeling and Artificial Intelligence in Ophthalmology*, vol. 2, no. 3, pp. 36–42, 2019.

[33] K. Riedlová, M. C. Saija, A. Olżyńska, P. Jurkiewicz, P. Daull, J.-S. Garrigue, and L. Cwiklik, "Influence of baks on tear film lipid layer: In vitro and in silico models," *European Journal of Pharmaceutics and Biopharmaceutics*, vol. 186, pp. 65–73, 2023.

[34] K.-H. Hsu, K. Gupta, H. Nayaka, A. Donthi, S. Kaul, and A. Chauhan, "Multidose preservative free eyedrops by selective removal of benzalkonium chloride from ocular formulations," *Pharmaceutical research*, vol. 34, pp. 2862–2872, 2017.

[35] L. Bräuer and F. P. Paulsen, "Tear film and ocular surface surfactants," *Journal of Epithelial Biology & Pharmacology*, vol. 1, no. 1, 2008.

[36] F. Rausch, M. Schicht, F. Paulsen, I. Ngueya, L. Bräuer, and W. Brandt, ""sp-g", a putative new surfactant protein–tissue localization and 3d structure," *PLOS ONE*, vol. 7, no. 10, pp. 1–13, 2012.

[37] F. Rausch, M. Schicht, L. Bräuer, F. Paulsen, and W. Brandt, "Protein modeling and molecular dynamics simulation of the two novel surfactant proteins sp-g and sp-h," *Journal of molecular modeling*, vol. 20, pp. 1–12, 2014.

[38] L. Braeuer, M. Schicht, and F. P. Paulsen, "Sp-g, a novel surfactant protein of the ocular surface that regulates surface tension of tears and might play a role in dry eye disease," *Investigative Ophthalmology & Visual Science*, vol. 60, no. 9, pp. 307–307, 2019.

[39] M. Schicht, K. Riedlová, M. Kukulka, W. Li, A. Scheer, F. Garreis, C. Jacobi, F. Paulsen, L. Cwiklik, and L. Bräuer, "The potential role of sp-g as surface tension regulator in tear film: From molecular simulations to experimental observations," *International Journal of Molecular Sciences*, vol. 23, no. 10, p. 5783, 2022.

[40] Y. J. Gordon, E. G. Romanowski, and A. M. McDermott, "A review of antimicrobial peptides and their therapeutic potential as anti-infective drugs," *Current eye research*, vol. 30, no. 7, pp. 505–515, 2005.

[41] S. S. Tummanapalli and M. D. Willcox, "Antimicrobial resistance of ocular microbes and the role of antimicrobial peptides," *Clinical and Experimental Optometry*, vol. 104, no. 3, pp. 295–307, 2021.

[42] D. Smajs, H. Pilsl, and V. Braun, "Colicin u, a novel colicin produced by shigella boydii," *Journal of bacteriology*, vol. 179, no. 15, pp. 4919–4928, 1997.

[43] H. Pilsl, D. Smajs, and V. Braun, "The tip of the hydrophobic hairpin of colicin u is dispensable for colicin u activity but is important for interaction with the immunity protein," *Journal of bacteriology*, vol. 180, no. 16, pp. 4111–4115, 1998.

[44] T. Dolejšová, A. Sokol, J. Bosák, D. Šmajs, I. Konopásek, G. Mikušová, and R. Fišer, "Colicin u from shigella boydii forms voltage-dependent pores," *Journal of Bacteriology*, vol. 201, no. 24, pp. 10–1128, 2019.

[45] A. J. Beevers and A. Kukol, "Transmembrane protein models based on high-throughput molecular dynamics simulations with experimental constraints," *Molecular Modeling of Proteins*, pp. 213–227, 2008.

[46] O. Guvench and A. D. MacKerell, "Comparison of protein force fields for molecular dynamics simulations," *Molecular modeling of proteins*, pp. 63–88, 2008.

[47] A. Hinchliffe, *Molecular Modelling for Beginners*. John Wiley & Sons, 2008.

[48] D. Chandler, "Introduction to modern statistical," *Mechanics. Oxford University Press, Oxford, UK*, vol. 5, no. 449, p. 11, 1987.

[49] E. R. Lindahl, "Molecular dynamics simulations," *Molecular modeling of proteins*, pp. 3–23, 2008.

[50] T. Róg, M. Girych, and A. Bunker, "Mechanistic understanding from molecular dynamics in pharmaceutical research 2: lipid membrane in drug design," *Pharmaceuticals*, vol. 14, no. 10, p. 1062, 2021.

[51] G. H. Grant and W. G. Richards, *Computational Chemistry*. Oxford Chemistry, Oxford University Press Inc, reprinted ed., 2005.

[52] S. Kmiecik, D. Gront, M. Kolinski, L. Wieteska, A. E. Dawid, and A. Kolinski, "Coarse-grained protein models and their applications," *Chemical reviews*, vol. 116, no. 14, pp. 7898–7936, 2016.

[53] C.-E. A. Chang, Y.-M. M. Huang, L. J. Mueller, and W. You, "Investigation of structural dynamics of enzymes and protonation states of substrates using computational tools," *Catalysts (Basel, Switzerland)*, vol. 6, no. 6, p. 82, 2016.

[54] H. I. Ingólfsson, C. A. Lopez, J. J. Uusitalo, D. H. de Jong, S. M. Gopal, X. Periole, and S. J. Marrink, "The power of coarse graining in biomolecular simulations," *Wiley Interdisciplinary Reviews: Computational Molecular Science*, vol. 4, no. 3, pp. 225–248, 2014.

[55] P. Kar and M. Feig, "Recent advances in transferable coarse-grained modeling of proteins," *Advances in protein chemistry and structural biology*, vol. 96, pp. 143–180, 2014.

[56] S. J. Marrink, H. J. Risselada, S. Yefimov, D. P. Tieleman, and A. H. De Vries, "The martini force field: coarse grained model for biomolecular simulations," *The journal of physical chemistry B*, vol. 111, no. 27, pp. 7812–7824, 2007.

[57] X. Shi and F. Tian, "Multiscale modeling and simulation of nano-carriers delivery through biological barriers—a review," *Advanced Theory and Simulations*, vol. 2, no. 1, p. 1800105, 2019.

[58] J. C. Phillips, R. Braun, W. Wang, J. Gumbart, E. Tajkhorshid, E. Villa, C. Chipot, R. D. Skeel, L. Kale, and K. Schulten, "Scalable molecular dynamics with namd," *Journal of computational chemistry*, vol. 26, no. 16, pp. 1781–1802, 2005.

[59] D. A. Case, T. E. Cheatham III, T. Darden, H. Gohlke, R. Luo, K. M. Merz Jr, A. Onufriev, C. Simmerling, B. Wang, and R. J. Woods, "The amber biomolecular simulation programs," *Journal of computational chemistry*, vol. 26, no. 16, pp. 1668–1688, 2005.

[60] B. R. Brooks, R. E. Bruccoleri, B. D. Olafson, D. J. States, S. a. Swaminathan, and M. Karplus, "Charmm: a program for macromolecular energy, minimization, and dynamics calculations," *Journal of computational chemistry*, vol. 4, no. 2, pp. 187–217, 1983.

[61] E. Lindahl, B. Hess, and D. Van Der Spoel, "Gromacs 3.0: a package for molecular simulation and trajectory analysis," *Molecular modeling annual*, vol. 7, pp. 306–317, 2001.

[62] D. Van Der Spoel, E. Lindahl, B. Hess, G. Groenhof, A. E. Mark, and H. J. Berendsen, "Gromacs: fast, flexible, and free," *Journal of computational chemistry*, vol. 26, no. 16, pp. 1701–1718, 2005.

[63] M. Abraham, D. van der Spoel, E. Lindahl, B. Hess, and the GROMACS development team, *GROMACS User Manual version 2019.6*, 2019. `http://www.gromacs.org`.

[64] W. F de Azevedo, "Molecular dynamics simulations of protein targets identified in mycobacterium tuberculosis," *Current medicinal chemistry*, vol. 18, no. 9, pp. 1353–1366, 2011.

[65] P. C. Biggin and P. J. Bond, "Molecular dynamics simulations of membrane proteins," *Molecular Modeling of Proteins*, pp. 147–160, 2008.

[66] J. A. Lemkul, "Gromacs tutorial - tutorial 1: Lysozyme in water." `http://www.mdtutorials.com/gmx/lysozyme/06_equil.html`. Access of the day: 31.3.2024.

[67] J. A. Lemkul, "From proteins to perturbed hamiltonians: A suite of tutorials for the gromacs-2018 molecular simulation package, v1.0," *Living Journal of Computational Molecular Science*, vol. 1, no. 1, p. 5068, 2018.

[68] D. J. Tobias, G. J. Martyna, and M. L. Klein, "Molecular dynamics simulations of a protein in the canonical ensemble," *The Journal of Physical Chemistry*, vol. 97, no. 49, pp. 12959–12966, 1993.

[69] O. M. Salo-Ahen, I. Alanko, R. Bhadane, A. M. Bonvin, R. V. Honorato, S. Hossain, A. H. Juffer, A. Kabedev, M. Lahtela-Kakkonen, A. S. Larsen, *et al.*, "Molecular dy-

namics simulations in drug discovery and pharmaceutical development," *Processes*, vol. 9, no. 1, p. 71, 2020.

[70] T. Karmakar, A. R. Finney, M. Salvalaglio, A. O. Yazaydin, and C. Perego, "Non-equilibrium modeling of concentration-driven processes with constant chemical potential molecular dynamics simulations," *Accounts of Chemical Research*, vol. 56, no. 10, pp. 1156–1167, 2023.

[71] D. H. De Jong, G. Singh, W. D. Bennett, C. Arnarez, T. A. Wassenaar, L. V. Schafer, X. Periole, D. P. Tieleman, and S. J. Marrink, "Improved parameters for the martini coarse-grained protein force field," *Journal of chemical theory and computation*, vol. 9, no. 1, pp. 687–697, 2013.

[72] S. J. Marrink and D. P. Tieleman, "Perspective on the martini model," *Chemical Society Reviews*, vol. 42, no. 16, pp. 6801–6822, 2013.

[73] A. Wizert, D. R. Iskander, and L. Cwiklik, "Organization of lipids in the tear film: a molecular-level view," *PLoS One*, vol. 9, no. 3, p. e92461, 2014.

[74] A. Wizert, D. R. Iskander, and L. Cwiklik, "Interaction of lysozyme with a tear film lipid layer model: A molecular dynamics simulation study," *Biochimica et Biophysica Acta (BBA)-Biomembranes*, vol. 1859, no. 12, pp. 2289–2296, 2017.

[75] S. M. Lam, L. Tong, B. Reux, X. Duan, A. Petznick, S. S. Yong, C. B. S. Khee, M. J. Lear, M. R. Wenk, and G. Shui, "Lipidomic analysis of human tear fluid reveals structure-specific lipid alterations in dry eye syndrome1 [s]," *Journal of lipid research*, vol. 55, no. 2, pp. 299–306, 2014.

[76] I. A. Butovich, "Tear film lipids," *Experimental eye research*, vol. 117, pp. 4–27, 2013.

[77] T. Viitaja, J.-E. Raitanen, A. Hynynen, J. Moilanen, K. Svedström, R. O. Paananen, and F. S. Ekholm, "On the importance of chain branching in tear film lipid layer wax and cholesteryl esters," *Colloids and Surfaces B: Biointerfaces*, vol. 214, p. 112429, 2022.

[78] A. H. Rantamäki, T. Seppänen-Laakso, M. Oresic, M. Jauhiainen, and J. M. Holopainen, "Human tear fluid lipidome: from composition to function," *PloS one*, vol. 6, no. 5, p. e19553, 2011.

[79] S. J. Marrink, A. H. De Vries, and A. E. Mark, "Coarse grained model for semi-quantitative lipid simulations," *The Journal of Physical Chemistry B*, vol. 108, no. 2, pp. 750–760, 2004.

[80] W. L. DeLano, "The pymol molecular graphics system," *http://www. pymol. org/*, 2002.

[81] W. Humphrey, A. Dalke, and K. Schulten, "Vmd: visual molecular dynamics," *Journal of molecular graphics*, vol. 14, no. 1, pp. 33–38, 1996.

[82] L. Martínez, R. Andrade, E. G. Birgin, and J. M. Martínez, "Packmol: A package for building initial configurations for molecular dynamics simulations," *Journal of computational chemistry*, vol. 30, no. 13, pp. 2157–2164, 2009.

[83] H. J. Berendsen, J. v. Postma, W. F. Van Gunsteren, A. DiNola, and J. R. Haak, "Molecular dynamics with coupling to an external bath," *The Journal of chemical physics*, vol. 81, no. 8, pp. 3684–3690, 1984.

[84] T. Castrignano, P. D. De Meo, D. Cozzetto, I. G. Talamo, and A. Tramontano, "The pmdb protein model database," *Nucleic acids research*, vol. 34, no. suppl_1, pp. D306–D309, 2006.

[85] W. Kabsch and C. Sander, "Dictionary of protein secondary structure: pattern recognition of hydrogen-bonded and geometrical features," *Biopolymers: Original Research on Biomolecules*, vol. 22, no. 12, pp. 2577–2637, 1983.

[86] M. Winterhalter, "Black lipid membranes," *Current Opinion in Colloid & Interface Science*, vol. 5, no. 3-4, pp. 250–255, 2000.

[87] J. Yang, R. Yan, A. Roy, D. Xu, J. Poisson, and Y. Zhang, "The i-tasser suite: protein structure and function prediction," *Nature methods*, vol. 12, no. 1, pp. 7–8, 2015.

[88] F. Sievers, A. Wilm, D. Dineen, T. J. Gibson, K. Karplus, W. Li, R. Lopez, H. McWilliam, M. Remmert, J. Söding, *et al.*, "Fast, scalable generation of high-quality protein multiple sequence alignments using clustal omega," *Molecular systems biology*, vol. 7, no. 1, p. 539, 2011.

[89] F. Sievers and D. G. Higgins, "Clustal omega, accurate alignment of very large numbers of sequences," *Multiple sequence alignment methods*, pp. 105–116, 2014.

[90] A. H. Delcour *et al.*, *Electrophysiology of unconventional channels and pores*, vol. 18. Springer, 2015.

[91] M. W. Parker, J. P. Postma, F. Pattus, A. D. Tucker, and D. Tsernoglou, "Refined structure of the pore-forming domain of colicin a at 2.4 å resolution," *Journal of molecular biology*, vol. 224, no. 3, pp. 639–657, 1992.

[92] J. L. Hilsenbeck, H. Park, G. Chen, B. Youn, K. Postle, and C. Kang, "Crystal structure of the cytotoxic bacterial protein colicin b at 2.5 å resolution," *Molecular microbiology*, vol. 51, no. 3, pp. 711–720, 2004.

[93] M. Wiener, D. Freymann, P. Ghosh, and R. M. Stroud, "Crystal structure of colicin ia," *Nature*, vol. 385, no. 6615, pp. 461–464, 1997.

[94] P. Elkins, A. Bunker, W. A. Cramer, and C. V. Stauffacher, "A mechanism for toxin insertion into membranes is suggested by the crystal structure of the channel-forming domain of colicin e1," *Structure*, vol. 5, no. 3, pp. 443–458, 1997.

[95] I. R. Vetter, M. W. Parker, A. D. Tucker, J. H. Lakey, F. Pattus, and D. Tsernoglou, "Crystal structure of a colicin n fragment suggests a model for toxicity," *Structure*, vol. 6, no. 7, pp. 863–874, 1998.

[96] T. Arnold, K. Zeth, and D. Linke, "Structure and function of colicin s4, a colicin with a duplicated receptor-binding domain," *Journal of biological chemistry*, vol. 284, no. 10, pp. 6403–6413, 2009.

[97] P. D. Bank, "Protein data bank," *Nature New Biol*, vol. 233, no. 223, pp. 10–1038, 1971.

[98] M. Olšinová, P. Jurkiewicz, I. Kishko, J. Sỳkora, J. Sabó, M. Hof, L. Cwiklik, and M. Cebecauer, "Roughness of transmembrane helices reduces lipid membrane dynamics," *Iscience*, vol. 10, pp. 87–97, 2018.

[99] K. Riedlová, T. Dolejšová, R. Fišer, and L. Cwiklik, "H1 helix of colicin u causes phospholipid membrane permeation," *Biochimica et Biophysica Acta (BBA)-Biomembranes*, vol. 1864, no. 4, p. 183866, 2022.

[100] S. Uran, Å. Larsen, P. B. Jacobsen, and T. Skotland, "Analysis of phospholipid species in human blood using normal-phase liquid chromatography coupled with electrospray ionization ion-trap tandem mass spectrometry," *Journal of Chromatography B: Biomedical Sciences and Applications*, vol. 758, no. 2, pp. 265–275, 2001.

[101] W. Dowhan, "Molecular basis for membrane phospholipid diversity: why are there so many lipids?," *Annual Review of Biochemistry*, vol. 66, no. 1, pp. 199–232, 1997.

[102] J. P. Jämbeck and A. P. Lyubartsev, "Derivation and systematic validation of a refined all-atom force field for phosphatidylcholine lipids," *The journal of physical chemistry B*, vol. 116, no. 10, pp. 3164–3179, 2012.

[103] J. P. Jambeck and A. P. Lyubartsev, "An extension and further validation of an all-atomistic force field for biological membranes," *Journal of chemical theory and computation*, vol. 8, no. 8, pp. 2938–2948, 2012.

[104] W. L. Jorgensen, J. Chandrasekhar, J. D. Madura, R. W. Impey, and M. L. Klein, "Comparison of simple potential functions for simulating liquid water," *The Journal of chemical physics*, vol. 79, no. 2, pp. 926–935, 1983.

[105] F. Chen and P. E. Smith, "Simulated surface tensions of common water models," *The Journal of chemical physics*, vol. 126, no. 22, 2007.

[106] A. A. Gurtovenko and I. Vattulainen, "Effect of nacl and kcl on phosphatidylcholine and phosphatidylethanolamine lipid membranes: insight from atomic-scale simulations for understanding salt-induced effects in the plasma membrane," *The Journal of Physical Chemistry B*, vol. 112, no. 7, pp. 1953–1962, 2008.

[107] L. X. Dang, G. K. Schenter, V.-A. Glezakou, and J. L. Fulton, "Molecular simulation analysis and x-ray absorption measurement of ca2+, k+ and cl-ions in solution," 2006.

[108] M. J. Abraham, T. Murtola, R. Schulz, S. Páll, J. C. Smith, B. Hess, and E. Lindahl, "Gromacs: High performance molecular simulations through multi-level parallelism from laptops to supercomputers," *SoftwareX*, vol. 1, pp. 19–25, 2015.

[109] K. Lindorff-Larsen, S. Piana, K. Palmo, P. Maragakis, J. L. Klepeis, R. O. Dror, and D. E. Shaw, "Improved side-chain torsion potentials for the amber ff99sb protein force field," *Proteins: Structure, Function, and Bioinformatics*, vol. 78, no. 8, pp. 1950–1958, 2010.

[110] M. Javanainen, "Universal method for embedding proteins into complex lipid bilayers for molecular dynamics simulations," *Journal of chemical theory and computation*, vol. 10, no. 6, pp. 2577–2582, 2014.

[111] B. Hess, H. Bekker, H. J. Berendsen, and J. G. Fraaije, "Lincs: A linear constraint solver for molecular simulations," *Journal of computational chemistry*, vol. 18, no. 12, pp. 1463–1472, 1997.

[112] B. Hess, "P-lincs: A parallel linear constraint solver for molecular simulation," *Journal of chemical theory and computation*, vol. 4, no. 1, pp. 116–122, 2008.

[113] S. Miyamoto and P. A. Kollman, "Settle: An analytical version of the shake and rattle algorithm for rigid water models," *Journal of computational chemistry*, vol. 13, no. 8, pp. 952–962, 1992.

[114] S. Nosé, "A molecular dynamics method for simulations in the canonical ensemble," *Molecular physics*, vol. 52, no. 2, pp. 255–268, 1984.

[115] M. Parrinello and A. Rahman, "Polymorphic transitions in single crystals: A new molecular dynamics method," *Journal of Applied physics*, vol. 52, no. 12, pp. 7182–7190, 1981.

[116] M. Abraham, A. Alekseenko, V. Basov, C. Bergh, E. Briand, A. Brown, M. Doijade, G. Fiorin, S. Fleischmann, S. Gorelov, G. Gouaillardet, A. Grey, M. E. Irrgang,

F. Jalalypour, J. Jordan, C. Kutzner, J. A. Lemkul, M. Lundborg, P. Merz, *et al.*, *GROMACS 2024.1 Manual*, 2024.1 ed., 2024. https://doi.org/10.5281/zenodo.10721192.

[117] U. Essmann, L. Perera, M. L. Berkowitz, T. Darden, H. Lee, and L. G. Pedersen, "A smooth particle mesh ewald method," *The Journal of chemical physics*, vol. 103, no. 19, pp. 8577–8593, 1995.

[118] K. Riedlová, M. C. Saija, A. Olżyńska, K. Vazdar, P. Daull, J.-S. Garrigue, and L. Cwiklik, "Latanoprost incorporates in the tear film lipid layer: an experimental and computational model study," *International Journal of Pharmaceutics*, vol. 645, p. 123367, 2023.

[119] G. N. Mathioudakis, A. Soto Beobide, G. Bokias, P. G. Koutsoukos, and G. A. Voyiatzis, "Surface-enhanced raman scattering as a tool to study cationic surfactants exhibiting low critical micelle concentration," *Journal of Raman Spectroscopy*, vol. 51, no. 3, pp. 452–460, 2020.

[120] H. Mochizuki, M. Yamada, S. Hatou, and K. Tsubota, "Turnover rate of tear-film lipid layer determined by fluorophotometry," *British journal of ophthalmology*, vol. 93, no. 11, pp. 1535–1538, 2009.

List of Abbreviations

APPL	Area per polar lipid
BAKs	Mixture of alkylbenzyldimethylammonium chlorides with alkyl chains ranging from C8 to C18
BLM	Black lipid membranes
BO	Behenyl oleate
CE	Cholesteryl erucate
CG	Coarse-grained simulations
CTD	C-terminal domain
FF	Force field
LTP	Latanoprost
MD	Molecular dynamic
MM	Molecular mechanic
PBC	Periodic boundary conditions
PDB	Protein Data Bank
PL	Polar lipids of TFLL
PME	Particle mesh Ewald summation
POPC	1-palmitoyl-2-oleoyl-sn-glycero-3-phosphatidylcholine
POPE	1-palmitoyl-2-oleoyl-sn-glycero-3-phosphoethanolamine
POPG	1-palmitoyl-2-oleoyl-sn-glycero-3-phospho-glycerol
SPs	Surfactant proteins
SP-G	Surfactant protein G
TF	Tear film
TFLL	Tear Film Lipid Layer
VdW	Van der Waals